Predicting Adsorbent Performance for Carbon Capture using Machine Learning Models

By

Terry Ming Yiu So

A thesis

presented to the University of Waterloo

in fulfillment of the

thesis requirement for the degree of

Master of Applied Science

in

Chemical Engineering

Waterloo, Ontario, Canada, 2023

Author's Declaration

I hereby declare that I am the sole author of this thesis. This is a true copy of the thesis, including any required final revisions, as accepted by my examiners.

I understand that my thesis may be made electronically available to the public.

Abstract

Carbon capture is a promising way to slow down climate change from anthropogenic sources. One of the carbon capture technologies that is being actively researched is adsorption. Given the increasing amount of literature that present novel ideas, being able to predict this information based on adsorbent textural properties is desirable. In this thesis, machine learning is used to construct a model to estimate adsorbent performance.

Currently, many groups are researching novel adsorbents simultaneously. While beneficial for development, the organization of data varies between papers, as preparation and testing conditions affect the adsorbent performance. Determining the adsorbent data representative of the adsorbent is a difficult challenge, given the presentation and availability are varied. Thus, a section of the thesis focuses on determining which parameters are able to represent the adsorbents while being commonly reported in the literature. A general review of the textural properties is presented. The adsorbent types are also described in the literature review to capture the differences present in adsorbents.

Models trained using five different machine learning methods are examined in detail. The models use the adsorbent's textural properties along with the testing conditions to estimate the adsorption capacity for an adsorbent. Additionally, the isotherm parameters are also targeted in additional models. Comparisons are performed between the directly predicted capacity and the capacity estimated from the modeled isotherm parameters; this is performed over the different machine learning methods used. A section of the thesis is dedicated to examining a sample adsorbent in more detail based on the ML model. An Aspen Adsorption bed model is used to investigate the effects of the differences between the model. The models exhibit limited performance in the general setting, despite the good training performance. The performance is approximate at a high level, but the requirements to capture the relationship between the adsorbents and its performance is not readily available.

Acknowledgements

I thank my supervisor Professor Ali Elkamel for his support and supervision during the process of the degree. He has graciously provided a position where I am fortunate enough to work. In addition, I have worked in collaboration with CANMET at Natural Resources Canada (NRCAN). They have provided their expertise and guidance that shaped the project. The collaboration works adjacent to this work with sections of each project drawing from the data set we have created.

Table of Contents

List of Figures

List of Tables

Chapter 1: Introduction

In this chapter, a general motivation and background pertaining to climate change is given. The objective of the thesis is also described thereafter.

1.1. Background

Climate change is increasingly becoming a major forefront of research and development. Multiple avenues are necessary to confront the ever-daunting task; research is conducted in areas such as producing clean energy, reducing consumption, and lowering waste production. Public awareness is gaining more momentum, as an increased demand for electric automobiles and renewable energy sources grow. However, this remains but one facet that is needed to mitigate climate change. In particular, reducing waste generated is connected to manufacturing and power generation sites. Enhanced efficiency towards reducing emissions benefits these companies as the government applies more pressure to reduce waste output.

A key target in this waste output is carbon dioxide. CO_2 is generated in a plethora of ways, but one that applies to manufacturers is burning fuel for power generation. Burning fuel produces flue gas, which contains CO_2 and other pollutants. Reducing CO_2 can either be done before, during or post fuel combustion. For existing sites, retrofitting a post-combustion capture system is the only economical option to come to newer standards.

Carbon dioxide can be captured and either utilized or sequestered; research, development, and integration fall under carbon capture, utilization, and sequestration (CCUS). While there are many methods of capturing carbon, adsorption is one with potential. The current economics and efficiency hamper the installation of adsorption units; the high costs currently outweigh the benefits. As more adsorbents approach the development stage, the exact connection between the sorbent design and the physical performances remains illusive.

Modeling with machine learning is capable of learning implicit or unidentifiable connections. These capabilities are penetrating many different fields, especially in engineering; in particular, ML models' ability to find these relationships make it fitting to connect the sorbent properties to its performance.

1.2. Objective

The objective of this thesis is described briefly in two parts.

- First, a data set is required to train the potential machine learning models. An existing data set that contains the necessary sorbent properties does not exist, requiring a general literature review to collect adsorbent information that is available but unorganized.
- Second, ML models are trained on this adsorption data set. The adsorption capacity, as the target variable, can be estimated either directly or by prediction using isotherm parameters. Isotherm parameters fitted from experimental data is found from the National Institute of Standards and Technology's (NIST) publicly available data base, which act as training data.

Ultimately, these two objectives are used to create conclusions on the application of machine learning technology on adsorption data, as well as the comparison between ML and the general isotherm model.

1.3. Outline

The thesis is organized in six chapters.

- Chapter 2: Literature Review

  Literature review is composed of several short sections that briefly describe carbon capture, adsorption, and machine learning.

  The first section describes the flue gas represented in the real application. The second section after describes carbon capture technologies, including adsorption and absorption. The chapter proceeds to a third section describing adsorption cycling. A fourth section is dedicated towards describing the different types of adsorbents available.

  The fifth and final section in this chapter goes over the machine learning algorithms at a high level.

- Chapter 3: Data Collection

  Chapter 3 covers the basis of the data collection in this context, including the parameters of interest as described by previous work, the different databases used, the lack of data consistency among the sorbents.

- Chapter 4: Aspen Adsorption Model

  This chapter describes the development of a process-level adsorption bed model, which represents a real-world cyclical system to be used to evaluate the performance of the machine learning models.

- Chapter 5: Machine Learning Models

  ML models trained on the data from Chapter 3 is developed throughout this Chapter 5. The chapter covers the first iteration using neural networks, the investigation into potential improvements, and additional development of models trained by other ML methods. The models are examined using the prior-developed bed model in Chapter 4.

- Chapter 6: Conclusion & Future Work

  Conclusions on the capabilities of ML with adsorption currently are drawn based on the results of Chapter 5. Improvements and future works are discussed, which is of importance to further develop a more cohesive landscape for adsorption in the future.

Chapter 2: Literature Review

In this chapter, a review of relevant literature is given to preface the model. Section 2.1 describes the different flue gases in industry. In section 2.2, adsorption, the CO2 separation technique used in this work, is described generally. Section 2.3 details the adsorption process from a process level. The adsorbents are also included in the review, in section 2.4. Finally, section 2.5 briefly covers the machine learning algorithms used for the necessary models.

2.1. Flue Gas

The properties of the flue gas are important in determining the design of the system, including the separation technology and choice of adsorbent. The differences for each flue gas originate from its combustion. The composition, temperature and pressure are dependent on the industry, the location of the combustion, the equipment involved and any specialized treatment that may be done.

The Government of Canada gathers data detailing the emissions from different manufacturers. The amount of greenhouse gases (GHG) emissions is aggregated and made publicly available online. A plot of the total GHG emissions in each industry over time is shown below. The tabulated data can be found in Appendix A.

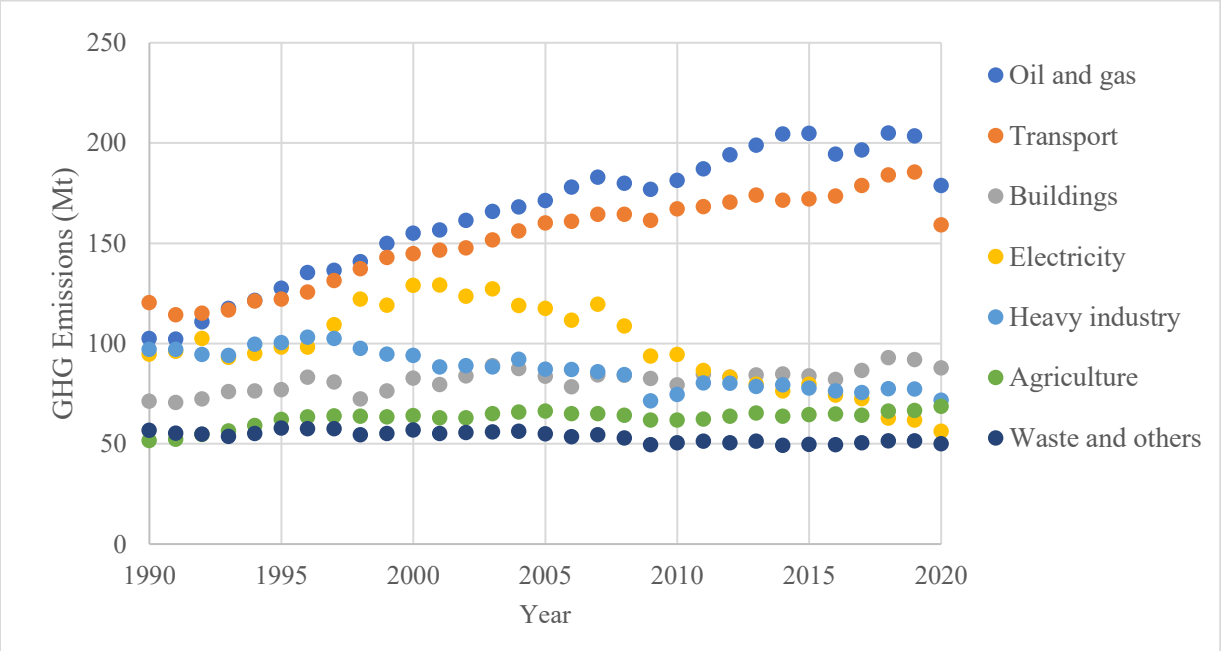

Figure 2.1: GHG Emissions over Time by Economic Sector in Canada [1]

The above figure shows that the oil and gas, electricity generation and heavy industry are three areas that produce a significant amount of GHG. These areas contribute to GHG from sources such as manufacturing, natural gas, power generation, and industrial, among others. Certain flue gases also have different compositions due to the combustion conditions. Biogas, biofuel, oxyfuel and syngas all contribute but these areas are separately considered compared to more typical combustion sources.

Another consideration for processing carbon is the effects of combustion. Different technologies work around the conditions of combustion to capture carbon in different situations. These technologies include pre-combustion, oxyfuel and post-combustion. Pre-combustion technology captures carbon from the fuel before combustion. A high concentration of oxygen contacts the fuel to produce a combination of CO and H_2 syngas; alternatively, steam reforming can also occur to produce a similar syngas product [2]. Oxidation and steam reformation are used together in auto-thermal reforming, which helps balance the opposing exothermic oxidation reaction with endothermic steam reformation. After impurities are removed, steam is introduced to engage the water gas shift reaction. The reaction produces CO_2 and H_2 gas by reacting CO and H_2O, concentrating CO_2 to be captured later. The fuel is converted to H_2 gas which converts to water when combusted. The CO_2 and H_2 gas must be separated before; this can be done by syngas scrubbing with amine-based solvents, or otherwise separated with compression, condensation, or flashing. Theoretically, pre-combustion can be cheaper up to 45% of post-combustion and 24% of oxyfuel combustion costs [2]. However, active plants usually have existing fuel combustion systems which make retrofitting pre-combustion technology expensive. Operation at the production level lacks technical knowledge for effective implementation [3].

Oxyfuel combustion introduces high concentrations of O_2 and recycled flue gas for a higher proportion of complete combustion. The products of oxyfuel combustion are primarily CO_2 and H_2O, which is easier to process than more typical combustion products such as CO and SO_x. While interest is growing in oxyfuel combustion, the largest challenge is supplying a high concentration of O_2. The separation of O_2 from air is expensive for economics and energy efficiency. Research is ongoing for O_2 separation, which includes developments as oxygen-transporting membranes that are difficult to upscale. Moreover, pilot systems are implemented and used to evaluate and demonstrate the feasibility; however, the required experience to run the process at an industrial level is rare.

2.2. Carbon Capture Technologies

There are a multitude of technology that are emerging and developing to be used for carbon capture. While some technologies are commercially available, more research and development are needed to increase the capture efficiency and economic viability for many of these technologies. Gas purification processes in general can be found as one of five categories; these categories are absorption, adsorption, membrane separation, chemical conversion, and condensation [4]. Absorption with liquid solvents, separation with membranes, biological conversion with living organisms and adsorption with solid sorbents are several techniques developed for CCUS. While the focus of this thesis is the adsorption process and solid sorbents, a high-level overview of the other technologies is first given for comparison.

2.2.1. CO2 Capture by Absorption

Absorption is a common separation technique to separate impurities in gas streams. Aside from post-combustion CCUS, other applications include hydrogen sulphide removal in refineries, ethylene oxide and acrylonitrile absorption in petrochemicals, and carbon dioxide absorption in water in food processing [5]. Absorption remains as one of the most developed carbon capture technologies, being implemented in commercial applications. This stems from the relative maturity of the technology; an early US patent for carbon dioxide capture using aqueous ammonia was initially filed in 1926 [6]. Continuous innovation and development throughout the years has made absorption a viable technology to mitigate carbon output.

Amine solvents are used in many absorption-based carbon capture processes. Monoethanolamine (MEA) is one of the most common solvents in absorption capture processes. Amine-based solvents are chemical solvents; chemical solvents depend on the reaction chemistry of the solvent, which pertains to operational considerations such as absorption capacity, kinetics, and presence of side reactions. Alternative to amine-based sorbents are physical sorbents, into which carbon dioxide dissolves; methanol is one example of a physical sorbent. The CO_2 solubility has a trade-off between low energy requirements for solvent regeneration, and greater dependence on flue gas temperature and pressure. The choice of solvent depends on numerous factors, such as flue gas conditions, utility availability and outlet requirements.

There are several major advantages of absorption, as evidenced from the real applications. The maturity of the process makes it technologically developed enough to be implemented in

processes today. For amine solvents, special care must be accounted for the additional corrosion. Factors such as higher loading, higher temperatures and the type of solvent all affect the corrosion rate in equipment [7]. The regeneration of chemical solvents can be expensive based as well and may increase with a higher flow rate for the flue gas or regeneration steam, as well as any low-pressure regeneration conditions.

2.2.2. CO_2 Capture by Membrane Separation

Membranes can be used to selectively separate carbon dioxide and other gases from the bulk flue gas. While other gases such as nitrogen and hydrogen remain on the flue gas side of the membrane, a selective membrane allows carbon dioxide to diffuse to the outlet side. Ideal traits for a selective membrane are having high permeability of CO_2 while maintaining high selectivity of other gases. The diffusion is driven by a pressure gradient; a high pressure on the inlet side and a low pressure on the outlet side promotes general gas permeation through the membrane. It is important to have specific membrane qualities depending on the flue gas composition. While high CO_2 permeability is desired, the composition of the flue gas heavily affects the requirements. For example, post-combustion membrane separation has higher nitrogen gas concentration, in comparison to separation from natural gases, which has a greater amount of methane [3]; membranes with high nitrogen gas selectivity may be unsuited for another process if methane permeation is an issue.

Membranes come in various categories depending on the structure of the membrane. As the name suggests, polymeric membranes are made from polymers; an example of polymeric membrane is polyethylene glycol (PEG) [3]. However, polymeric membranes may encounter CO_2 plasticization at higher pressures. When plasticization occurs, a gas modifies the membrane's physical structure where it is dissolved in the membrane surface, potentially affecting parameters important to membrane operation. The rate of plasticization is promoted as higher pressures and higher carbon dioxide concentrations. Plasticization has varying effects, both positive and negative, on permeability, which depends on opposing factors of diffusivity at higher pressure and solubility at the membrane [8].

In contrast to polymeric membranes, inorganic membranes separate carbon dioxide based on their textural properties. The pore channels can restrict certain gases from permeating through the membrane, acting as a molecular sieve for separation [3]. Certain membranes also exhibit high selectivity for CO_2 depending on its affinity. An example of inorganic membranes is zeolite

membrane; zeolites such as zeolite imidazolate frameworks (ZIF) have been involved in the development of novel mixed matrix membranes (MMM), where a polymeric membrane and other membranes combine to improve overall performance [9].

An advantage of membrane is that the process unit is relatively simple, compared to absorption or adsorption units. The operation of absorbers and adsorbers require a method of regeneration, such as cyclical staging of multiple units. While maintenance is still required for membrane units, the same is true for sorbents, or other technologies in general. As well, the process time and process flow rate of sorption-based technology compared to permeation in membranes should be compared. However, the disadvantages of membranes include the membrane cost being notably high and the outlet purity of a single membrane is relatively low; the low purity can be partially mitigated with recycle streams. However, both the membrane cost and the presence of a recycle stream make it currently economically unviable for larger processes [3]. As more research is conducted to reduce the cost and increase the efficiency, the strong advantages of membrane units may be more viable and easier to implement.

2.2.3. CO_2 Capture by Biological Conversion

Interest has gained for biological conversion of carbon dioxide in various research studies. One of the potential organisms that can facilitate biological conversion is microalgae. While informally, microalgae are generally understood to be all algae that cannot be seen without additional equipment, there is no unifying definition to group microalgae [10].

The use of microalgal growth is the basis of CO_2 removal through conversion. Microalgae have different types of growth that use carbon differently. Photoautotrophs use photosynthesis to convert CO_2 into organic matter. Heterotrophic growth requires organic carbon instead but does not require sunlight or other radiant energy for conversion. Mixotrophic uses a staged combination of both heterotrophic and autotrophic growth depending on the conditions; autotrophic growth is preferred in the presence of organic carbon while autotrophic growth becomes more dominant in the absence of organic carbon [3]. Each growth types have different trade benefits and detriments. The light requirement of autotrophic growth is an extra factor to operate, control and expense, while heterotrophic growth has a lower rate of carbon dioxide conversion.

Differences arise between more traditional carbon capture technologies and microalgae. Post-capture operations in CCUS are an important consideration, which has an impact on the design and objectives of the system. For non-biological processes, a common CCUS method is to

pressurize the capture CO_2 to the liquid phase for better transport. For biological conversion, carbon dioxide is instead converted to biomass. This biomass has other uses in nutrition, pharmaceuticals, fertilizers, and other products [3]. Another advantage is that microalgae are usable for a broad range of carbon dioxide. While higher concentrations affect the biomass growth rate, microalgae can be used to capture carbon dioxide directly from air; absorption and adsorption can have issues targeting direct air capture applications due to the low concentration and low driving force for the processes. However, a major drawback in using microalgae is the operating cost is relatively high. This is due to the stricter control for optimal capture rate in biomass systems. Control of the temperature, pH, flow rate and other gases is required to prevent loss in efficiency or, with poorly optimized systems, cell death.

2.2.4. CO_2 Capture by Adsorption

Another prospective technology is carbon capture via an adsorption process. Adsorption is a phenomenon where particles in a fluid phase adsorb onto a catalyst surface. At the molecular level, adsorbate particles react at specific active sites on the catalyst surface. The active site depends on the surface of the catalyst; certain active groups may be present to bond with the adsorbate molecule. This bonding may either be physical or chemical. The rate of adsorption is dependent on the number of active sites available; this, in turn, is related to the surface area accessible to adsorbate particles.

There are different types of adsorptions based on how the sorbate and sorbent interact. Chemisorption occurs when the sorbate chemically bonds with the sorbent. A high heat of adsorption and high energy requirements for reversing sorption reaction is typical given the strong chemical bonds binding the sorbate and sorbent. As well, interactions are more specific. From a molecular perspective, a particle can react with the adsorbent if it collides with an active site with a particle amount of energy and orientation; these interactions will have greater specificity based on the sorbate, as well as create a dependency on the process conditions [11]. In contrast, physisorption has no chemical bond between sorbate and sorbent; instead, weaker intermolecular forces form the bond. The weaker forces result in contrasting features to chemisorption. A low heat of adsorption, lower regeneration requirements, faster kinetics and less selectivity is generally expected for physical adsorbents. Both types of adsorbents are used but many physisorption features align with the requirements of carbon capture. Low heat of adsorption requires less temperature control. Favourable regeneration can be used to easily remove carbon dioxide for

storage or utilization and regenerate adsorbents. Fast kinetics indicate less adsorbent and smaller units may be possible. All of these factors depend on the adsorbent itself, including its adsorption capacity, heat of adsorption and reaction kinetics.

Adsorption kinetics are modeled in a variety of methods. While specific pore modelling is a possibility, adsorption isotherms are more introductory and easily applicable at the industrial level. Isotherms relate the equilibrium adsorption capacity and the sorbate concentration; the sorbate pressure or concentration are used in isotherms depending on how the isotherm is defined. Some isotherms can be formed based on kinetics on a molecular level, which depend on certain assumptions. The assumptions affect the accuracy depending on the adsorbent as assumptions. Alternatively, empirical isotherms can be fitted based on experimental data. Combining aspects of the empirical isotherm with a more theoretical approach may also fit certain adsorbents better.

A simple theoretical model commonly used in adsorption models is the Langmuir isotherm, proposed by the eponymous Irving Langmuir in 1918 [12]. The derivation is commonly described as an introduction to adsorption processes. The isotherm assumes that the reaction is proportional to the fraction of active sites that are available; the derivation begins as a series of elementary reactions. At equilibrium, the forward and reverse reaction rates are equal, which is used to determine the fraction of occupied sites. Upon rearranging, the isotherm can be derived with two constant parameters, given below:

$$\Gamma_L(p) = \Gamma_{L\infty} \frac{K_L p}{1 + K_L p}$$

The maximum adsorption capacity $\Gamma_{L\infty}$ is the amount of adsorbate that can be maximally adsorbed per mass of sorbent. The equilibrium constant K_L loosely describes the rate of forward and reverse reaction rates. The equation is expressed in terms of sorbate partial pressure p, at the catalyst surface. This theoretical example makes several assumptions. First, the molecules interact with the catalysts only at the active sites. Second, the active site interacts with one sorbate particle. Third, each active site is equally favourable. Fourth, each adsorbed molecule does not affect other molecules' interactions [11]. These assumptions, while they can be applied to many sorbents, are not necessarily valid. In particular, neighbouring molecules may interact with each other, especially with larger molecules that sterically hinder each other. Similarly, adsorbents do not necessarily create a monolayer of adsorbed species. The intermolecular interactions can cause

adsorbate to form multiple layers. Nonetheless, the simplicity and general applicability of the Langmuir isotherm makes it one of the most common isotherms to use.

The Freundlich isotherm is based on a combination of empirical and analytical assumptions. The derivation of the isotherm notices that the heat of adsorption decreases as more active sites are filled. It is assumed that this is decreases logarithmically. Simplifying this assumption sufficiently presents the isotherm as follows:

$$\Gamma_F(p) = k_F p^{\frac{1}{n_F}}$$

Given the empirical nature of this equation, the parameters k_F and n_F do not explicitly represent physical terms. However, an increase in temperature leads to a decrease in k_F and an increase in n_F; this also agrees with a lower adsorption capacity at higher temperatures.

Both the Langmuir and Freundlich isotherms model certain adsorbents better than the other model. Combining the two models creates a hybrid model that combines the theoretical features of the Langmuir isotherm with the more empirical fit from Freundlich isotherm. This Langmuir-Freundlich isotherm is shown below:

$$\Gamma_{LF}(p) = \Gamma_{LF\infty} \frac{(K_{LF}p)^{n_{LF}}}{1 + (K_{LF}p)^{n_{LF}}}$$

This equation can have improved fitting over both the Langmuir and Freundlich isotherms. Graphically, the general curve for Langmuir and Freundlich isotherms cannot change, which does not agree with some experimental adsorption processes; combining these features and having an extra degree of freedom can increase the fitting. In the below figures, two isotherms from the collected data set are depicted that exhibit relatively poor fitting for either the Langmuir or Freundlich isotherm. In comparison, the other isotherms, including the Langmuir-Freundlich isotherm, exhibits better fitting. Below, two sets of adsorption data are shown; the three adsorption isotherms described above are fitted to the datasets.

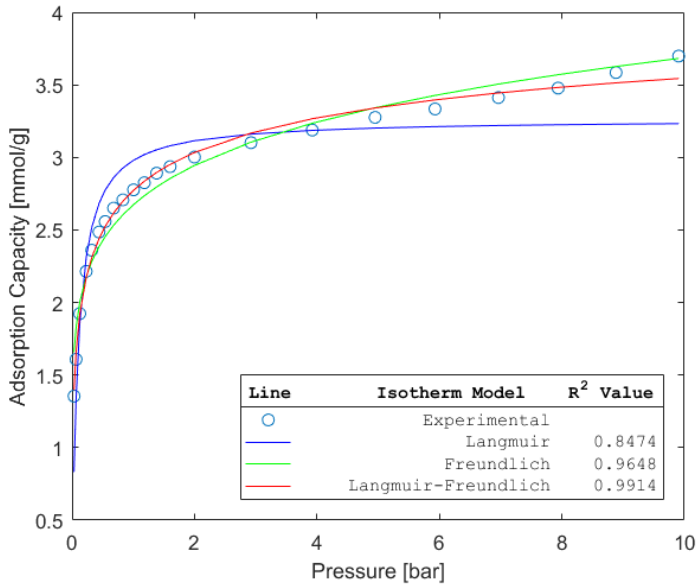

Figure 2.2: Adsorption Isotherm for Zeolite 5A at 323 K [13]

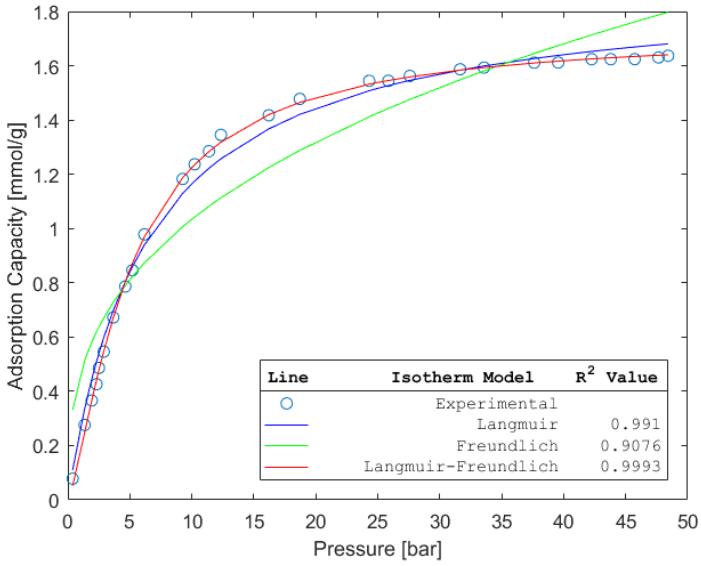

Figure 2.3: Adsorption Isotherm for SNU-50 at 298 K [14]

In the above Figure 2.2, the Langmuir isotherm has low fitting compared to the Freundlich and Langmuir-Freundlich isotherms. The lower R^2 value of 0.8474 is reflected in the deviations that are exacerbated at the higher pressures; the Langmuir isotherm underestimates the growth of the adsorption capacity for zeolite 5A. While the cause of the difference can be the result of many different factors, this can be due to the Langmuir isotherm assumptions being invalid. Additional

interactions and adsorbate layers can increase the capacity more than predicted. In comparison, the adsorption equation for SNU-50 has relatively poor fitting for the Freundlich isotherm, while the Langmuir isotherm has better performance. As the Freundlich isotherm is only experimental, the cause of the discrepancy may be more difficult to determine. Graphically, the Freundlich isotherm underestimates the capacity between 5 and 35 bars, and otherwise overestimates the capacity. The Freundlich isotherm fitting for SNU-50 shows the opposite issue as before, where the exponential term does not fit to the high growth rate at low pressures and lower growth rate at high pressures. Both of the adsorption data, however, have good fitting for the combined Langmuir-Freundlich isotherm equation. The combination match both the Langmuir and Freundlich's relations shown by either adsorbent, partially helped by the additional degree of freedom compared to the two-parameter isotherms. Thus, if the fitting is available, using the Langmuir-Freundlich isotherm can be good for fitting different adsorbent behaviour with one equation. Other adsorption isotherms also exist with benefits and assumptions, but the focus is directed towards these three isotherms mentioned.

2.3. Adsorption Process

On the process unit level, adsorption can take place in one of several unit configurations. One of the most common is the fixed bed. The bed is filled with adsorbent particles, where the flue gas passes through; for carbon capture systems, treated flue gas passes through the bed of adsorbents to release low carbon dioxide effluent. The equations governing a fixed bed are well known, which is preferred for testing performance. The adsorbents are loaded with sorbate until the loading at the end of the bed is close to equilibrium. The sorbent must be regenerated. This is done by swing adsorption; these regenerative steps use the effects of pressure and temperature on adsorption equilibrium to control CO_2 adsorption and desorption.

Pressure swing adsorption (PSA), as the name suggests, uses pressure to control adsorption and desorption. In general, increasing the overall pressure promotes adsorption. Thus, PSA has the adsorption step performed at higher pressure and the desorption at lower pressure. A simple four-stage cycle, known as the Skarstrom cycle, is shown in Table 2.1; the valves indicated in the table for each step are opened while the remainder of the valves are closed. The accompanying Figure 2.4 shows a flow sheet for the table. The Skarstrom cycle is shown as four stages that are staggered between the two columns. For Column 1, the first stage in the cycle is the feed stage; feed gas

comes into Column 1, has carbon dioxide adsorbed from the gas, and exits lean on CO_2. The next stage is blowdown, where the gas in column 1 is vented. The carbon dioxide adsorbed in the feed and pressurization steps desorbs during this step, due to the decrease in pressure from the venting. The third step, purge, further removes the adsorbed carbon dioxide by recycling part of the gas from Column 2 into Column 1. The recycle gas, lean on CO_2, promotes the desorption reaction rate. Once the adsorbent is sufficiently unloaded, Column 1 can begin the pressurization step, which begins to fill with flue gas. This is then cycled into the feed step, while Column 2 operates similarly to achieve continuous operation.

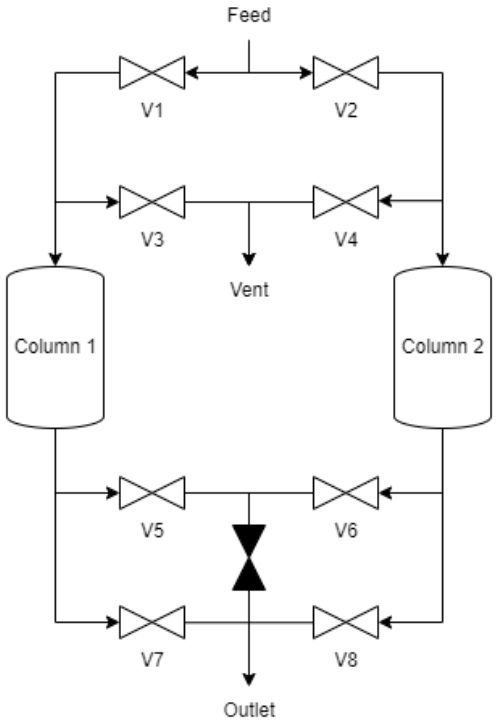

Figure 2.4: Simple Diagram for Skarstrom Cycle

Table 2.1: Valve Staging for Skarstrom Cycle

Column	Stage 1	Stage 2	Stage 3	Stage 4
Column 1	Feed	Blowdown	Purge	Pressurize
	V1, V7	V3	V5. V3	V1
Column 2	Purge	Pressurize	Feed	Blowdown
	V4, V6	V2	V2, V8	V4

The Skarstrom cycle given above is possible for a two-bed design. However, improvements in efficiency and flow rates can be achieved with additional process design decisions. Increasing the number of columns allow more flexibility in staging; other designs for the timing & staging and valve locations can affect equipment sizing, maximum flow rate and effluent purity. The design balances between the operational goals and the cost of additional design, both economically and operationally. This simple cycle also demonstrates the driving forces through PSA. The high concentration and pressurization drive the adsorption in Column 1 in stages 1 and 4, while the low concentration and pressure drive the opposite reaction. PSA's desorption pressure can also be extended to lower than atmospheric pressure. Vacuum pressure swing adsorption (VPSA) operates on the same principles as PSA. Instead, the pressure difference is in comparison with low pressures during regeneration, while PSA has high pressures during sorption While there are major advantages for regeneration in VPSA, the additional cost of operating a vacuum must be worked around. In particular, the cost of vacuum is highly dependent on the volume of flue gas that must be adsorbed [3].

Temperature swing adsorption (TSA) works similarly but uses a difference in temperature to drive the desorption. As adsorption is an exothermic process, the adsorption steps should be kept at a lower temperature, typically around 40°C [3]. Desorption is kept at higher temperatures over 100°C instead. Typically, this is done by using hot purging gas, such as steam. However, the heat transfer and desorption rates are long, which requires design considerations when planning the staging of TSA systems. An alternative method of heating the adsorbents is with electric swing adsorption (ESA). The catalyst has an electric current passed through it, which heats the catalyst to the desired temperature by the Joule effect. This bypasses the slow heat transfer between a hot purge gas and the adsorbent in typical TSA systems; instead, the temperature increases quickly through ESA [15]. In contrast, TSA can heat the purge gas using waste heat from the remainder of the system for better system efficiency. The electric power from ESA is not recycled but can still be used for processes without the excess heat required for TSA. Another challenge to using ESA is the adsorbent choice. Directly heating the adsorbent with electricity requires good conductivity to allow heating to the end of the bed. Indirectly heating the adsorbent with an instrument adjacent to the catalyst is also possible but introduces extra design and control elements [16].

These process cycles depend on relatively basic principles to control the equilibrium of the adsorption reaction to adsorb and desorb carbon dioxide as required. Combining pressure and

temperature effects can further change the equilibrium and increase the equilibrium driving force behind the reaction; however, the cost of these systems cannot be ignored, as more complex cycles can introduce more obstacles. Obstacles can include separating CO_2 from the purge gas in TSA cycles, or the increasing cost of inducing a vacuum during VPSA.

2.4. Adsorbent Types

As mentioned before, adsorption depends on process parameters such as pressure and temperature; however, a large factor is the adsorbent properties and structure. The textural properties of the sorbents have major effects and can also affect side-product formation in the presence of non-CO_2 species in the flue gas. Similar physical and textural properties can be used to group similar adsorbents. Adsorbents are grouped into the following groups: carbon-based, ceramic, metal oxide, metal organic framework (MOF), porous organic polymer (POP), silica, and zeolite. A brief description of the carbon-based, MOFs, POPs and zeolites are given.

2.4.1. Carbon-Based Adsorbents

While different carbon-based adsorbents exist, the most popular are activated carbons. These sorbents are relatively cheap due to its cheap production process. Activated carbons can exist as coke by-products, as well as produced from easily accessible materials such as bamboo and other organic matter. Activated carbons are physical adsorbents with relatively low adsorption capacities compared to specially designed adsorbents. However, the combination of easy production and regeneration make it a potential adsorbent. Aside from activated carbon, other carbon-based adsorbents such as nanocarbons and graphite can act as physisorbents for carbon capture. Development in nanocarbon and carbon-based adsorbents for carbon capture usage is relatively limited compared to more popular adsorbents such as metal organic frameworks or zeolites.

2.4.2. Metal Organic Frameworks

Metal organic frameworks (MOFs) are crystalline materials that are formed from both metallic and organic compounds, as the name suggests; metal clusters are held together with organic linkages. Metal nodes linked by organic linkages create a secondary building unit, which can be used as a building unit for larger crystal structures. MOFs can be specially modified to achieve certain features and enhance desired interactions; modifications can change the pore

structure & active sites and allow MOFs to be used for a variety of functions, such as gas storage, separation and chemical catalysis [17]. Alternatively, modifications to enhance CO_2 interactions with the sorbent is desired for MOFs and can be achieved by design. Specific design for CO_2 adsorption can increase the capacity and overall performance beyond other types of adsorbents. The synthesis of MOFs is particular in order to achieve certain properties. Factors such as temperature and solvent can affect the MOF's topology; in particular, controlling the synthesis reaction temperature controls the degree of the reaction as well as any potential side-reactions. This can change the dimensionality and density of the framework.

2.4.3. Porous Organic Polymers

Porous organic polymers (POPs) are frameworks of organic compounds. POPs can be either crystalline or amorphous. Crystalline POPs are organized similar to MOFs; while MOFs are metal compounds bonded by organic linkages, POPs consist of monomers bonded via a polymerization reaction [18]. Monomers greatly affect the resultant POP based on the polymer's functional groups and spatial orientation when bonding. This results in different bonding or restricting interactions with certain reactants. Properties such as pore sizes can change based on the size and functional groups of the monomer and resulting building unit. Given the complex interactions that occur when synthesizing POPs, an initial foray into polymer design is difficult; knowledge based on existing topologies and their interactions can help predict the resultant POP structure. Typically, two-dimensional POPs are more common whereas three-dimensional POPs require rarer three-dimensional monomers.

2.4.4. Zeolites

Zeolites are porous crystalline aluminosilicates, constructed from a crystal lattice of SiO_4 and AlO_4 molecules. The tetrahedron molecules are connected by shared oxygen atoms to form the lattice. The crystal lattice creates pores of distinct and uniform dimensions, in contrast to other porous media with varying pore distributions. Each zeolite is comprised of units of SiO_4 and AlO_4; while the Si/Al ratio is never less than one, the presence of aluminium introduces negative charges into the framework, which are balanced by cations in the pore space. The number of cations affect the carbon dioxide adsorption of zeolites; other factors affecting adsorption are the pore structure, and its subsequent effect on the electric field characteristics in the zeolite.

One of the major factors affecting the viability of zeolite is the presence of water. Water preferentially bonds to zeolite adsorption sites compared to carbon dioxide. Some zeolites, such as NaX zeolite, have increased adsorption capacities with the presence of water; however, the enhancement of the adsorption was only present for a select concentration range for carbon dioxide. At concentrations above 1,000 ppm CO_2, the loading begins to be lower than the dry NaX loading [19]. Moreover, the level of water concentration would also affect the adsorption enhancement. Excess amount of water can bind preferentially to the adsorption sites over CO_2, lowering the adsorption capacity. Controlling the water and carbon dioxide tightly to benefit from this enhancement can be difficult in larger scale facilities; as well, not all zeolites can benefit from the presence of water. Thus, the choice of zeolites should be considered more carefully if the presence of water is expected.

2.4.5. Other Adsorbents

Other adsorbent types are available outside of the four types covered in the above sections. Metal oxides are formed between a metal element and oxygen and contain sites that interact and bind with CO_2. Alkali earth and alkaline metal oxides are common metal oxides that adsorb carbon dioxide, but more exotic oxides are also capable. These adsorbents are chemisorbents and chemically bond with carbon dioxide; as mentioned above, this results in certain properties such as having a relatively highly exothermic heat of adsorption and higher regeneration requirements for desorption. For alkaline earth metals, the general reaction occurs as follows:

$$MO_s + CO_{2\,(g)} \leftrightarrow MCO_{3\,(s)}$$

Certain materials also possess mesoporous structures, when the pore sizes are between 2 nm and 50 nm [20]; in comparison, zeolites are considered to be microporous with less than 2 nm while sorbents with greater pore sizes can be considered as microporous. Many sorbents have pore sizes within the mesoporous range; prospective materials include ceramics and silica-based sorbents. Ceramics encompass a wide variety of materials; while the definition may not be universally defined, one definition used is a non-metallic inorganic solid. Silicates and other silicon-based materials are a critical section of ceramics. Silicates are abundant and naturally occurring, which can be useful in large-scale implementations. However, benefits from specially designed sorbents as POPs or MOFs will enable better performance.

2.5. Machine Learning Models

Machine learning as a concept has become incredibly popular within the recent decade, having breached both the mainstream and niche spaces. While general machine learning is a recent concept under development in the public space, machine learning has continuously been developed for a long time, with popular cultural implementations such as the chess computer Deep Blue developing in the 1980s. Machine learning predates such cultural breaches by several decades, with publications such as On Game-Learning Machines by Paul I. Richards in 1952.

As the name suggests, machine learning programs are programmed to learn from training examples to complete a function. Traditional programming requires more explicit algorithms that are consciously implemented; however, if a pattern is unknown or obtuse, machine learning can identify and approximate the function. In this thesis, the connection between the adsorbent properties and the adsorption capacity is difficult in both not explicitly known and difficult to implement. As adsorption is a surface phenomenon, modelling at the molecular level is required but requires higher levels of precision that may not work for every adsorbent. Given this, machine learning remains as a potentially viable method to connect the adsorbent to its capacity.

2.5.1. Neural Network

An introduction of machine learning models will certainly include neural networks. A neural network is a collection of nodes or neurons that are connected to apply many successive transformations. Each node applies a weight and bias to transform the input into an output. The nodes can be arranged in a series of layers; each layer is connected in sequence so that the intermediate outputs from the previous layer's nodes are used as inputs. A visual diagram of a neural network is shown below. The figure represents a neural network that attempts to predict the desired objective on the left. An input of various known conditions including temperature, pressure, surface area and pore volume are input into the model. Each of the nodes in the first hidden layer gather the inputs, which are subsequently transformed and fed into the third layer. The second hidden layer transforms these intermediate values and outputs another intermediate value. The sum of these intermediate values is used as the model's output. The weights and biases in the hidden layer are adjusted based on the training data set.

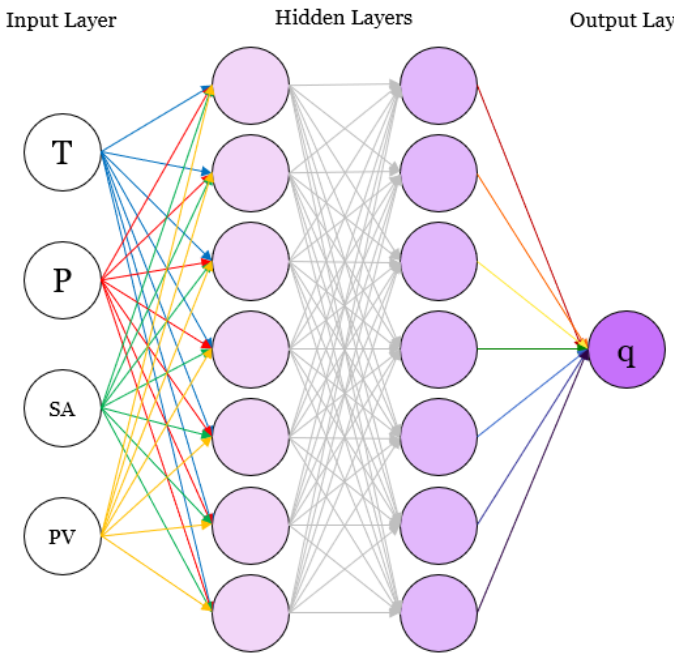

Figure 2.5: Visualization of a Neural Network

Optimizing the neural network can involve changing the structure of the network. These hyper parameters can change the performance of the model. The depth of the network describes the number of neurons in each layer, while the width of the network defines how many neurons are in a layer. In theory, a model with one sufficiently wide layer can estimate almost any function; the Universal Approximation Theorem indicates that shallow neural networks would be enough to estimate the adsorption performance. In practice however, deeper neural networks can have superior performance, within reasonable depth. Thus, changing both of these hyper parameters is necessary to create more representative neural networks.

In MATLAB, shallow neural networks can be created using the train function. The train function accepts inputs of a structured network object, the training inputs, the target values, input & layer delay conditions, and error weights. For a shallow neural network, the delay conditions are not used as there is only one hidden layer. Optionally, the network can be set up using the nftool function, where a user can set up the model using a wizard. This leads the user through choosing the training inputs and outputs, sorting the data into training, validation and testing sets, the number of neurons in the one hidden layer, and the training algorithm. After training the setting up and training the model, the user can choose to generate the equivalent code and save the results.

Different algorithms can be used to train the network. MATLAB has different choices, which can be changed depending on the dataset and the relationship. The algorithm used for this work is the Levenberg-Marquardt (LM) algorithm. Also known as damped least squares, the LM algorithm acts similarly to the Newton's method, with an additional term λ to compensate for the slow convergence when the extrema are far. When the model is closer an extreme point, λ is small and the algorithm is approximate to Newton's method. A large value of λ converts the equation to the equation for gradient descent. This enables the algorithm to quickly direct towards the extreme value using gradient descent, and then have more precise changes using the Newton's method. This algorithm is only valid for minimizing sum of squares because of the Jacobian term. MATLAB uses the mean square error as an indicator for network performance.

2.5.2. Regression Ensemble

Apart from neural networks, MATLAB contains other machine learning methods. While users can implement ML scripts similar to other programming languages, MATLAB also has built-in functions for certain algorithms. An example is the fitrensemble function, which use ensemble learning to train a regression model to target training output values. Ensemble models aim to develop weak learners, and then use the weak learners to estimate the target. The type of ensemble learning used in the function is automatically set to "LSBoost" or least-squares boost. For regression models, "Bag" or bootstrap aggregation is the alternative type of ensemble.

Boosting aims to uses the responses of weak learners to estimate the target response; for regression, the target is a target variable, but boosting can also be used for classification problems. The learners individually do not necessarily have good prediction performance, but the combination of learners contribute to the estimate [21]. For LSBoost, the learners are fitted to minimize the mean-squared error. Thus, each subsequent learner works towards the least-squared error of the combination of learners.

Bootstrap aggregation or bagging averages several bootstrap samples that are fitted to the model. Thus, the individual variance of the samples is reduced compared to the aggregate variance. Bootstraps draw samples from data sets to approximate the population. Samples are drawn and returned to the original data set, which allows samples to be chosen multiple times. MATLAB selects the algorithm choice of either LSBoost or Bag and assesses both when determining the best model.

2.5.3. Generalized Additive Model

Generalized additive models (GAMs) can also be generated from MATLAB's built-in functions. GAMs are models composed of a sum of univariate functions of the predictors. Thus, GAMs are represented by the equation below:

$$Y = \alpha + \sum_{j=1}^{p} f_j(X_j) + \varepsilon$$

Where Y is the response estimate, α is a constant, $f_j(X_j)$ are the univariate function of the predictors X_j, and ε is the error term. Different algorithms exist to estimate the functions of the GAMs, which have the appropriate weaknesses. For example, the backfitting algorithm uses cubic splines to fit to the target function. The process can be repeated until the new estimates satisfy a given threshold [21].

MATLAB's built-in function fitrgam uses LSBoost algorithm to fit a GAM. The function creates predictor trees for each predictor. Interactions between predictors are also represented by trees; bivariate functions can also be implemented in GAMs. The LSBoost algorithm, described above, is used and the response-aggregate predictor residual is minimized. When adding additional univariate trees does not improve the function, interaction terms are trained; when the function is not improved with additional interaction trees, fitrgam stops.

2.5.4. Gaussian Process

Gaussian process (GP) is a process that selects a sample from a population of models. One way to describe GPs is to consider a population of models separate from the data. While infinite number of these models exist, only a selection of these models may correspond to a given data set; Bayes' theorem can be used to limits the populations to a subset of models that better represent the data. These functions are multivariate functions that aim to target specific data. To select the best function, a kernel function is considered; at a high level, the kernel function measures the similarity of the inputs, as controlled by its definition and corresponding hyperparameters. GP then considers the targets of the model and selects functions that based on the combination of kernel and outputs; this selects a model from the population of models given a select sample of inputs.

GPs can then be represented by a model with uncertainty represented by a collection of acceptable functions. The variance is dependent on the hyperparameters chosen which can control the overall model.

2.5.5. Support Vector Machines

Support vector machines (SVMs) are more typically used for classification problems. When the dataset can be partitioned into two distinct sections, then a boundary can be established between the partitions. The boundary aims to have the largest margin between the two sections, measured from both sides. However, there may be data points between the partitions that make a clean partition not realistic. By strictly adhering to the boundary, a model may either not exist or be overly complex. Instead, slack variables can be introduced, where datasets can enter a marginal space while still being satisfactory for each partition [21]. This would be a typical implementation of SVMs for classifying data.

The principle of SVMs can be used to create a regression model. While SVM classifiers work around marginal points using slack variables, the analogous SVM regression model provides slack to points with a small residual; that is, if the residual is absolutely less than a given marginal value, then the loss function for that data point is zero. The slack value can yield models that estimate the overall trend better compared to a model with zero slack that overfits to the training data. However, if the slack value is too large, the model does not perform any meaningful modelling and instead causes the model to be too lenient for errors.

Chapter 3: Data Collection

To accomplish the data collection of adsorption data, the performance and relevant parameters of adsorbents was determined. Adsorbent performance can be characterized in different methods. A review by Patel, Byun and Yavuz addresses six checkpoints that effective adsorbents would aim to fulfill for cost-effective deployment [22]. The six checkpoints are as follows: have CO_2 adsorption capacity greater than two mmol per g of sorbent; be usable for over one thousand cycles; have a selectivity of 100 CO_2/other gases; be stable in various conditions such as temperatures of over 150°C, and in presence of H_2O, SO_x. and NO_x; have a sorbent cost of less than 10 USD/kg; and have a reaction rate of over one mmol/g/min. Each of the six checkpoints addresses one of the design obstacles encountered. Based on these checkpoints, data is appropriately taken from various sources in literature.

One of the prerequisites of making any model is to have a representative data set; this is especially important for machine learning models, where the data set needs to be both large and representative. Currently, literature contains summary and review papers that highlights adsorbents and innovations relating to the adsorption process. As the focus of these review papers are on the trends at the time of publishing, the collected data for adsorbents are relatively simple and usually only detail the adsorption capacity of the adsorbents. For example, in a review paper by Choi *et al*., they describe the different types of adsorbents and some of recent adsorbents' results [19]. The summary tables in the table include the temperature, pressure, testing method and adsorption capacity. Similarly, a review paper by Pardakhti *et al*. have varying amounts of data in their tables [23]. Some tables report physical properties such as the surface area and pore volume along with the adsorption capacity, as seen in their table describing ordered mesoporous carbons and carbon-based materials. Other tables provide only the temperature and pressure conditions with the adsorption, which is not suitable for additional data gathering.

It is common for the summary papers to detail the temperature, pressure and select adsorbent properties; these properties include the adsorption capacity and the selectivity of CO_2 or CH_4 against N_2. Thus, to get more detailed information, each reference is checked for additional information. The original papers can provide more detailed information on the surface area, pore volume, pore and micropore diameter, heat of adsorption, adsorption capacity and selectivity. However, most references are not uniform in their description. Instead, a mixed collection of data

is available in each reference. For adsorbent properties, the surface area and the adsorption capacity are the most common reported variables. The remainder of the variables often are not reported in a similar consistency. This is highlighted in the below table showing the initial raw data set gathered from the sources.

Table 3.1: Number of Raw Data Points Gathered from Literature Sources

Variable	Adsorption Capacity	BET Surface Area	Pore Volume	Micropore Volume	Pore Diameter	Heat of Adsorption
Number of Data Points	561	522	369	188	252	185

The table above shows the other parameters are not reported in a comparable frequency to the adsorption capacity. When considering the data points including the pore volume, the remainder of the data points do not necessarily correspond; in the subset of the 369 data points including the pore volume, the corresponding micropore volume or pore diameter data may not be available. Thus, the availability of data points is a problem.

Another obstacle is to ensure the data are comparable to each other. The surface area can be measured and described as either the Langmuir or the BET surface area. Papers frequently report the BET surface area over the Langmuir surface area, which makes it used for the data set assembled. The adsorption capacity can also be described in mmol/g or in other units, which may require the molar mass of adsorbent.

The importance of features in the adsorption process has been previously examined in a previous paper by Zhu *et al* [24]. In the paper, they describe the critical factors in determining the adsorption capacity for porous carbons. The factors are examined in a correlation matrix and with graphs showing the relative contribution for each feature at different temperature and pressures. In the correlation matrix, the adsorption capacity was most heavily affected by the temperature and pressure. The other properties examined include textural properties, including the BET surface area, pore volume and mesopore volume, and the chemical composition.

Despite the direction the correlation matrix emphasizes, the issues of data collection are due to the uniformity of the data presented in each paper. Each paper presents the adsorption capacity data; this is given as the papers are collected from a summary paper that lists them. However, the other adsorbent properties are not shared between the properties. While the micropore and ultra-micropore volumes are among the critical factors affecting the adsorption capacity, often only the

mesopore volume is presented. This creates an issue where, in the dataset, there are data points that have all of the data required, and some data points with none of the requisite data. The easiest solution is to only incorporate the data shared among all of the data points but that creates a data set that cannot represent the adsorbent properly; the remaining parameters at this point are the adsorption capacity, temperature and pressure which is not sufficient in estimating adsorbent characteristics.

Two additional data sources are also available that may potentially improve the data set. One of these sources of data is the Computational Simulations of MOFs for Gas Separations (COSMOS), a database of MOFs that have been refined to materials that can adsorb CO_2, N_2, and CH_4. This refinement is performed by calculating adsorbent properties, including the pore-limiting diameter and accessible surface area, among other factors using Zeo++. A filter is placed such that the before-mentioned adsorbates are able to enter the pores and access surface areas in the remaining adsorbents. This is combined with the Cambridge Structural Database, which provides details at the unit cell level, including cell angles and cell density. Unfortunately, the surface area as described by the COSMOS paper is not available. For future work, allowing this simulation data can greatly supplement the data, especially for the numerous MOF data that is available.

The second data set that is available is the NIST's adsorption data resource. This is a combination of search engine of curated adsorption data. This provides a valuable resource to find adsorbents that adsorb CO_2; the original paper can be later checked to see if sorbent information is available. However, another capability of the data base is the presence of isotherm data. The isotherm data provides a wide variety of temperatures and pressures obtained from the papers; NIST has a built-in fitting function for the three Langmuir, Freundlich and Langmuir-Freundlich isotherms described in section 2.2.4. By recording the isotherm parameters, additional variables are available for later use.

Combining these resources and performing the necessary filtering to restrict the influence of outlier points, a smaller data set is generated. This data set contains 2,125 data points of adsorbents at different process conditions. Given the limitations of the data set, the surface area and the pore volume are taken as the structural properties. Additionally, all three isotherm parameters are included and available. Further adding variables to this set results in massively restricting the size of the set. Data imputation on the pore diameter is performed with extremely poor results; the lack of complete data makes simulating the data within the system not feasible.

Chapter 4: Aspen Adsorption Model

To supplement the machine learning model, an adsorption unit is developed and modeled; the additional model aims to cover and evaluate the results of the machine learning models. The machine learning models aim to model behaviour at a small-scale, where adsorbent's structure has a direct impact; in comparison, a model for the adsorption unit would model at the process level. While the objective of the model is to represent an adsorption process unit, any potential future work will be done in Aspen HYSYS, in collaboration with NRCAN.

To model an adsorption unit, different software are evaluated to determine their abilities. Several software come from the Aspen software suite; this allows the use of pre-built packages and models to be used. As communicating with Aspen HYSYS is preferable, Python is initially considered but not ultimately used. While Python allows a greater degree of control, programming this to an equivalent level of detail as the equivalent model in the Aspen framework would be more difficult, especially as future projects may require additions that Aspen is more capable to handle. This is more notable when working with different property packages and components, which are more naturally implemented in Aspen software but must be manually implemented in more self-contained programming. Thus, the adsorption unit was not modeled in Python.

Within the Aspen suite, there are several applications that can be used to represent an adsorption unit. The two software are Aspen Custom Modeler (ACM) and Aspen Adsorption. While AspenPlus has the capability to represent an adsorber as a component separator, the level of detail is not sufficient. As this model is used in conjunction with the result of the machine learning models, the model should be able to change based on the adsorbent used; this primarily incorporates the isotherm characteristics of the adsorbent.

In ACM, users initialize a worksheet similar to AspenPlus, where the components and methods are chosen. The software also provides a variety of familiar equipment for users to implement in their process, such as pumps, compressors, and piping. The largest difference is the ability of users to create custom models from Aspen's framework. Custom models are able to receive material and energy streams, perform calculations based on a user's code and then output corresponding streams that can be user by other equipment.

Aspen Adsorption has a similar interface as ACM. The initialization of the components and methods are chosen identically; in addition, more common equipment are included and functional.

However, instead of custom models, Aspen Adsorption has more detailed adsorption equipment. Users can choose beds, void tanks, and valves specifically for the appropriate gas or liquid fluid. The bed model, in particular, has advanced settings specific for adsorption processes; Appendix E includes screenshots of the settings used, which include options for momentum and energy balances, kinetic models and adsorption isotherm.

In consideration of both software, ACM's flexibility is shown in one of the publicly available programs. The Carbon Capture Simulation for Industry Impact ($CCSI^2$) is a collaboration project that develops CCS models. $CCSI^2$ has participation from academic and national labs and industry partners; among their project, the organization has developed a Process Models Bundle that is available on their GitHub that uses ACM. The Process Models Bundle includes a Bubbling Fluidized Bed reactor, which is developed based on an amine-impregnated sorbent NETL32D [25]. While the model works well in the pre-determined scope of the $CCSI^2$ project, generalizing the models illustrates the difficulties in using ACM. Adjusting the models includes adding more gas components, implementing more generalized adsorption kinetics, and have better integration with the remaining components. However, ACM is sensitive to degrees of freedom; additional components added require additional equations that are not necessarily incorporated to the degrees of freedom calculation satisfactorily. In addition, $CCSI^2$ has component-specific equations such as the component diffusivity. While determining and adding equations is easy, the software, or user, can have difficulty in tracking the degrees of freedom, which results in a model that cannot be run and is difficult to debug. For the adsorption kinetics, the original model uses the rate laws for NETL32D. Having a generalized rate law would not be possible or accurate for most adsorbents. In other general models, the rate of adsorption is driven by a linear driving force; the rate of adsorption is then proportional to the difference between the current adsorbed amount and the equilibrium amount. Implementing this separate rate of adsorption changes how the adsorption is calculated, whose implementation is not straightforward. Finally, the integration with the remaining components is not possible for the given level. For a fluidized bed, there is a constant stream of sorbents that are passed through the reactor. The regeneration of the sorbents is not possible without implementing a separate custom model; the sorbents are user-defined and cannot be used with any other built-in units.

Aspen Adsorption has much better integration with the adsorption process, as the software is built specifically to simulate adsorption. However, the weakness of Aspen Adsorption is how it

is typically run in transient state. This is more accurate as the process runs from a new state to a cyclical steady state, but the software comes with a long runtime. Running one cycle of a process can exceed 5 minutes; this is especially difficult during program development, where the initial transient phase runs well but a user is more interested at another point in the process. As the runtime of the program continues, the program runs more slowly; this is further exacerbated for adsorbents with lower rates of adsorption. However, the model can still be run well and, given how the software is designed specifically for adsorption simulation, Aspen Adsorption was used to simulate the adsorption process unit.

The following figure below shows the Aspen Adsorption bed model. The adsorption bed parameters are adapted from Ntiamoah *et al.*'s work [26]. In the paper, the model uses a more specific dual-site Langmuir model for the sorbent NaUSY. In addition, the paper identifies several cycles that can occur.

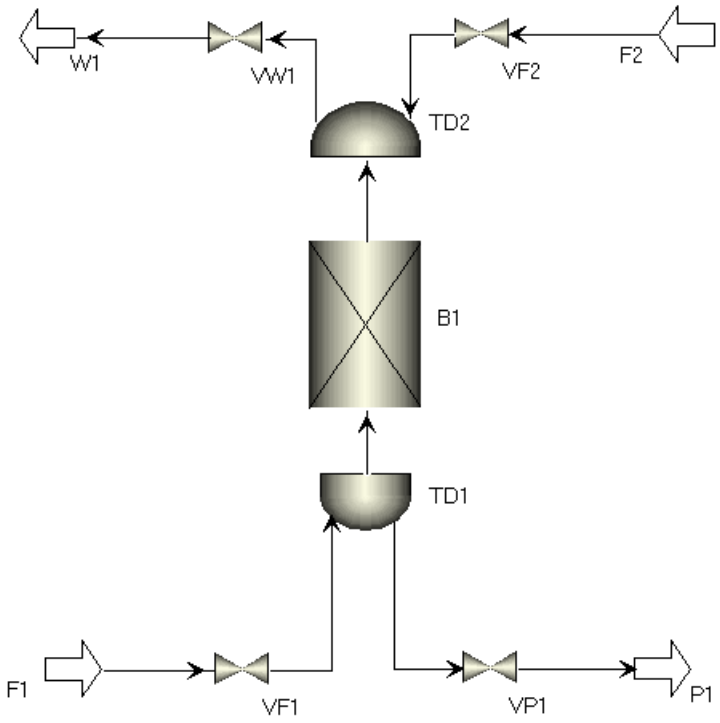

Figure 4.1: Diagram of Aspen Adsorption Bed Model

The model is a single-bed packed adsorption bed. The model considers four gaseous species: CO_2, N_2, H_2O, and O_2. In literature, adsorbents designed for carbon capture typically have isotherms available for CO_2 and N_2. The other two species are treated as inert; however, it is noted

that certain adsorbents such as zeolites have considerable interaction with water. This requires specific treatment for a particular interaction.

One of the advantages of Aspen Adsorption is the ability to implement a cycle, which is more typical of an adsorption unit. The cycle is adapted from the three-step Cycle 3 from Ntiamoah *et al.*'s paper. The steps of the cycle are feed (I), hot gas purge (III), and cooling (IV); the indirect heating (II) step is removed to improve the stability of the model. The cycle parameters are shown in the table below.

Table 4.1: Cycle Settings for Aspen Adsorption Model

Step	Feed (I)	Hot Gas Purge (III)	Cooling (IV)
Purpose	Adsorb CO_2 from feed gas	Regenerate adsorbents and recover CO_2	Remove CO_2 from bed and return temperature close to ambient
Conditional Trigger	$Y_{W1,\,CO2} > 0.05$	Same time length as Feed (I)	$Y_{W1,\,CO2} < 0.02$
Valve VF1	Open	Closed	Open
Valve VW1	Open	Closed	Open
Valve VF2	Closed	Open	Closed
Valve VP1	Closed	Open	Closed
Other	F1 set as feed gas		F1 set as pure N_2 gas

In the feed step, the feed gas from F1 enters the bed from the bottom. The temperature and pressure are ambient, while the flow rate, controlled by a feed valve VF1, is manually controlled to . The flue gas passes through the column and, the CO_2 and N_2 is adsorbed onto the unsaturated adsorbent. When the effluent product W1 has a CO_2 mole fraction of 0.05, the step is terminated. This indicates that the breakthrough for carbon dioxide has occurred, and the adsorbent is saturated with carbon dioxide. In the original paper, the mole fraction before termination is set to 0.03. A slightly higher mole fraction is chosen to increase the slack for the last step in the cycle.

The hot gas purge (III) step initially starts the regeneration process. The valves VF1 and VF2 are closed, while the hot gas purge valve VF2 and product valve VP1 are opened. The bed is fed hot gas counter-currently from . The hot gas composition is equivalent to the gas condition at the end of feed gas (I); this represents the configuration where the stream W1 is heated to 150°C and becomes the purge gas, which can be seen in multiple bed configurations. Instead of a conditional

trigger, the timing of the step is equal to the length of step 1. Previously, the trigger is based on the temperature at the bottom of the bed; when the temperature of the bottom of the column increases to the hot gas purge's temperature, then the step would terminate. This would simulate as a temperature breakthrough, equivalent to the first step's concentration breakthrough. In simulations, the heat of desorption and heat conduction in the fluid causes the temperature to behave differently than the equivalent concentration breakthrough; the temperature reaches the breakthrough temperature in a much shorter amount of time, which results in insufficient regeneration.

The last step is the cooling step (IV), which aims to bring the bed into a state where adsorption can begin again. This is done by purging the bed with N_2 gas at ambient temperature. The pure nitrogen gas purges the remaining CO_2 from the bed, while the elevated column temperature is lowered by the lower purge gas' temperature. The step and the cycle stop when the outlet CO_2 mole fraction of W1 decreases to 0.02. When this occurs, the bed is mostly unloaded of CO_2, and the temperature is equal to the ambient temperature as well. The adsorption bed is then ready for a new cycle to start capturing carbon.

To check the differences between the model in literature and the created model, a comparison between the breakthrough curves can be done. As not all parameters are presented in the paper, differences in certain assumptions change the breakthrough curve. Several parameters that are not explicitly stated are the feed valve flow rate setting, the jacketed heat exchanger settings such as the heat duty, cooling water flow rate or heat exchanger configuration, and the surrounding environment temperature. The temperature profile is affected by the heat exchanger settings, but the breakthrough may be affected by the flow rate and other factors.

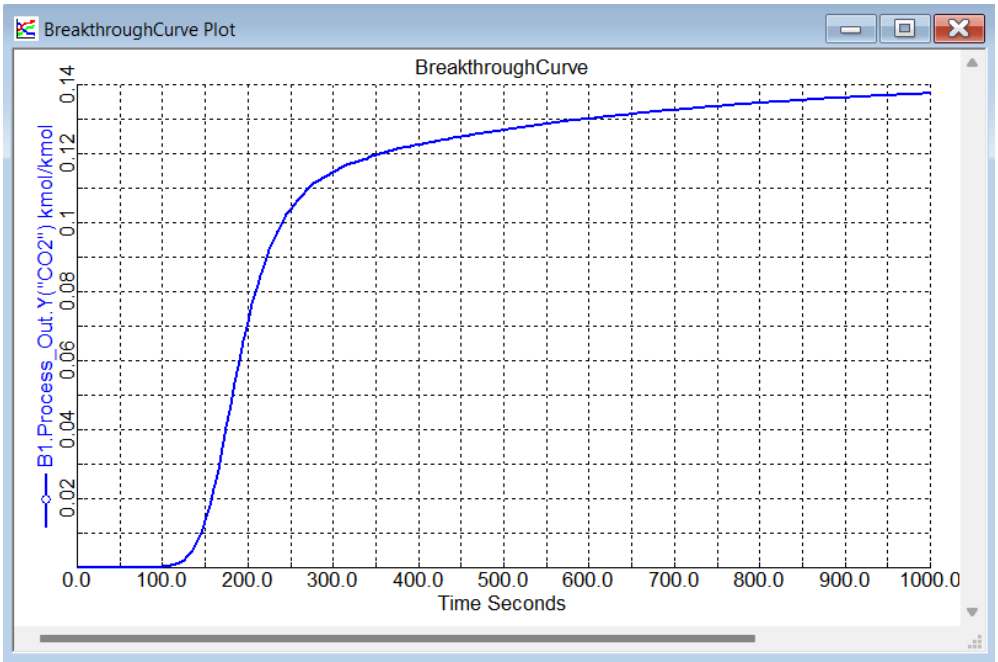

Figure 4.2: Breakthrough Curve for Simulated Aspen Adsorption Model using Approximated NaUSY Sorbent Parameters

Figure 4.2 shows the model can exhibit a typical breakthrough curve. The curve plots the outlet mole fraction of CO_2 in a time plot. When the model is initially running for approximately 100 seconds, the exit concentration does not change. The inlet concentration of CO_2 is adsorbed along the bed and does not penetrate the bed, until breakthrough where the concentration increases at the exit. The breakthrough point differs from the paper, which has a breakthrough point of approximately 250 seconds. This is controlled by the gas flow rate and velocity, as well as the inlet pressure from TD1. While the gas velocity is stated to be 0.42 m/s in their work, the inlet pressure is not stated, whereas the gas flow rate is estimated based on the gas flow rate. The valve control is measured in molar flow rate; equating the molar flow rate to the gas velocity makes assumptions that can change the column response. The original dual-site Langmuir isotherm is also changed to a single-site Langmuir isotherm, which changes the kinetics and transient gas distribution in the column. In addition, the reference model has an inert layer and an active layer. The inert layer adds an additional 0.2 m at the beginning of the unit. This creates an additional small delay, as the gas is slowed by the non-adsorbing material. However, the inert nature and short length relative to the velocity indicates that the contribution to this discrepancy may be limited. Overall, the Aspen Adsorption model yields comparable results to the model in the paper; the differences are attributed to the inlet conditions of the flue gas which is not explicitly stated in the reference paper.

Chapter 5: Machine Learning Models

The objective of the model is to predict the adsorption capacity, given the initial inputs described above. This differs from the more standard isotherm by allowing the capacity to be predicted from the adsorbent properties. Physical experiments to measure the adsorption capacity is an additional barrier to against quick research and development of new materials. Adsorbents that are prepared differently may exhibit different properties with different capacities; instead of multiple capacity measurements, the adsorption can be predicted. This allows researchers to determine which material and preparation are hopeful, which can streamline and focus the direction towards investigating the materials. A simpler machine learning model is initially implemented to investigate the performance.

Predicting the adsorption capacity using models can be done both directly and indirectly. A direct prediction indicates that the models output the adsorption capacity itself. Indirectly predicting the adsorption capacity requires target parameters used to predict capacity. Given that the collected data includes the experimentally fitted isotherm parameters from the NIST adsorption database, ML models can be trained to target the isotherm parameters and used to predict the capacity given certain pressure and temperature conditions. Thus, additional models are prepared to target the parameters for the Langmuir, Freundlich and combined Langmuir-Freundlich isotherms. The outputs of the models are unscaled based on the original data range, and then used as a parameter for the isotherm equation, along with the reported pressure.

A shallow neural network is created with the objective of outputting the target adsorption capacity, given the input data of BET surface area, pore volume, temperature and CO_2 pressure. The network is done using the trainlm function. Thus, four models are prepared for the adsorption capacity, and the three above-mentioned isotherms. Each parameter in the isotherms is independently trained in a neural network. Regression plots are prepared and shown below. The data points compare the experimentally determined adsorption capacity, with the predicted adsorption capacity; the data points are scaled based on the original adsorption capacity. Simple statistic diagnostics are also presented here.

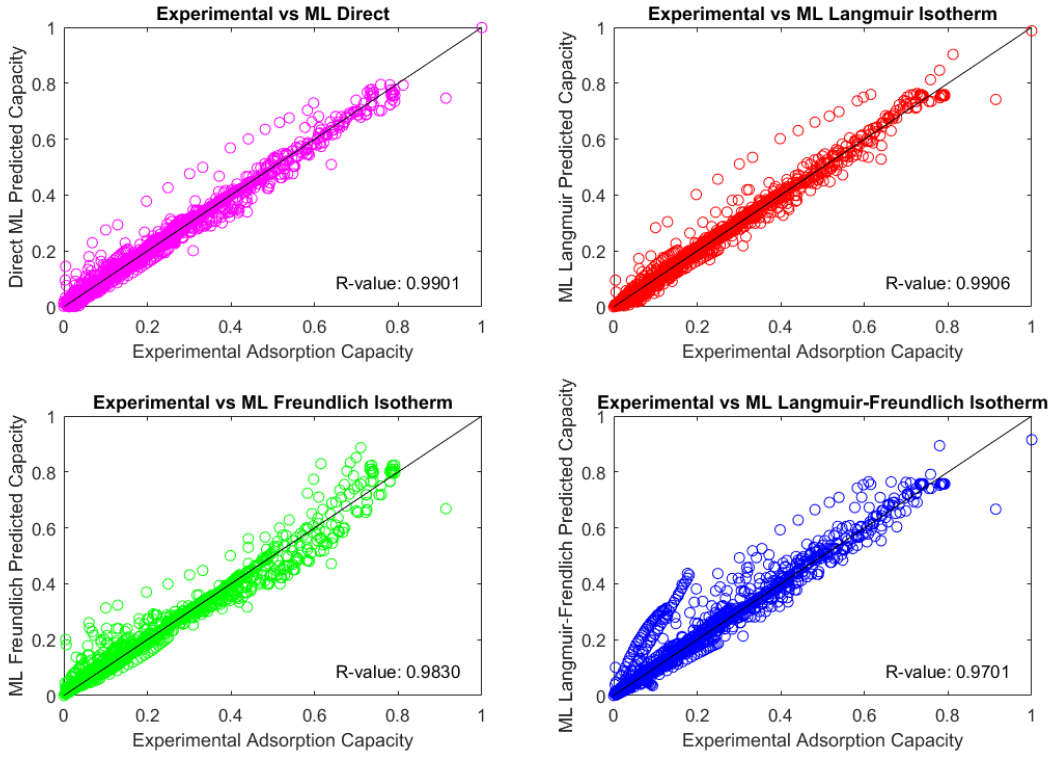

Figure 5.1: Regression Plots for Adsorption Capacity Models using Shallow Neural Networks

The neural network for the direct prediction is represented in the magenta plot at the upper left regression plot. This shallow neural network consists of 20 neurons. The neural network shows a large amount of correlation in the regression plots, with a calculated correlation coefficient of 0.9901. Graphically, the majority of points fall upon the desired line. However, there is a line of points in the plot that underestimate the capacity. Given that these points span along the capacities from 0.1 to 0.6 at the x-axis, it is an adsorbent that does not match with the remaining points. The other plots in Figure 5.1 also exhibit similar behavior. These outliers may be due to a sorbent that share similar characteristics with each other in terms of properties; however, the adsorption function may be different, which is not reflected in the inputs. There is not graphically discernable pattern, indicating that additional parameters are not necessary. An error histogram, shown below, does not show a regular pattern. The error histogram has twenty bins and aggregates errors outside of 1 mmol/g.

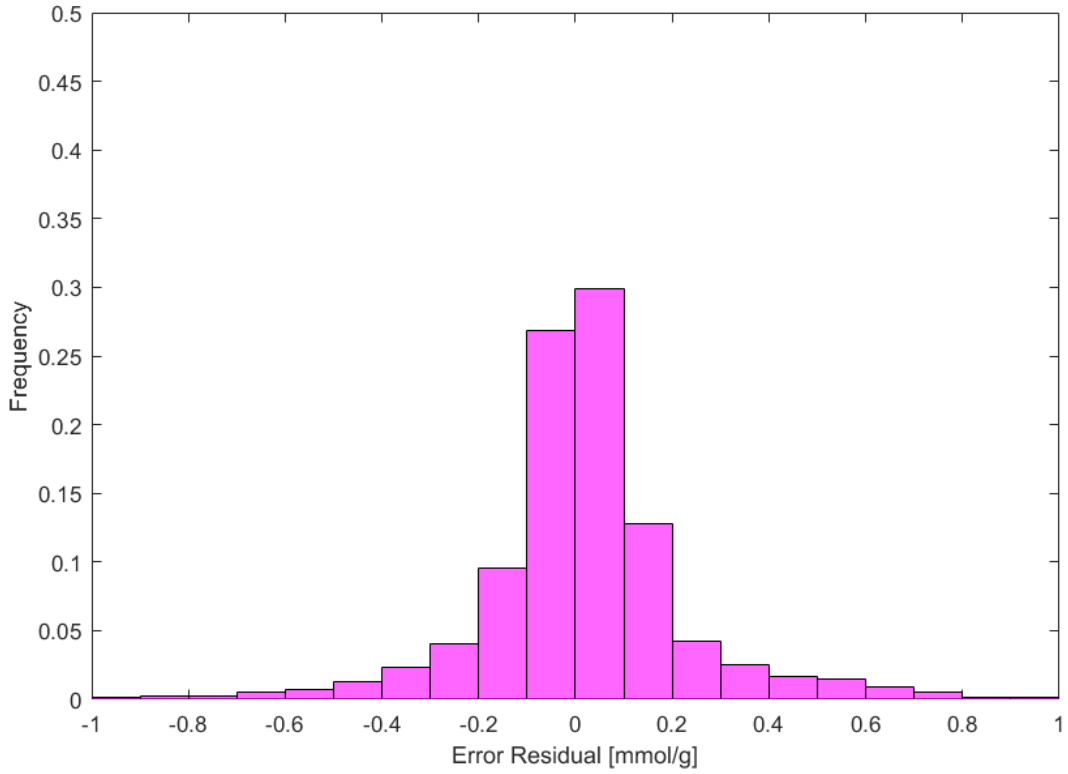

Figure 5.2: Error Histogram for Direct Adsorption Capacity Prediction with Shallow Neural Network

The error histogram shows a normal histogram curve, with the errors centered at the zero error. The aggregate bins at the curve extremities are small suggesting there are few extreme outliers. The bin containing errors between +0.1 to +0.2 mmol/g has a higher frequency then its corresponding negative bin, due to the line of outliers seen in the regression plot. A table is presented below with the R-values for the model; the overall R-value, as well as the R-values for the training, validation and testing datasets are shown. All of the R-values are greater than 0.98, showing that the model is a good fit for the dataset.

Table 5.1: R-Value and MSE for Shallow Neural Network Models

Model	Training R-Value	Validation R-Value	Testing R-Value	Overall R-Value	Overall MSR
Direct Prediction	0.9901	0.9923	0.9802	0.9901	0.0768

The model represented in the upper right plot in Figure 5.1 represents the model for the Langmuir isotherm. The isotherm consists of two isotherm parameters, each modeled by a shallow neural network. Both networks have fourteen neurons. Regression plots for the individual parameters are shown below.

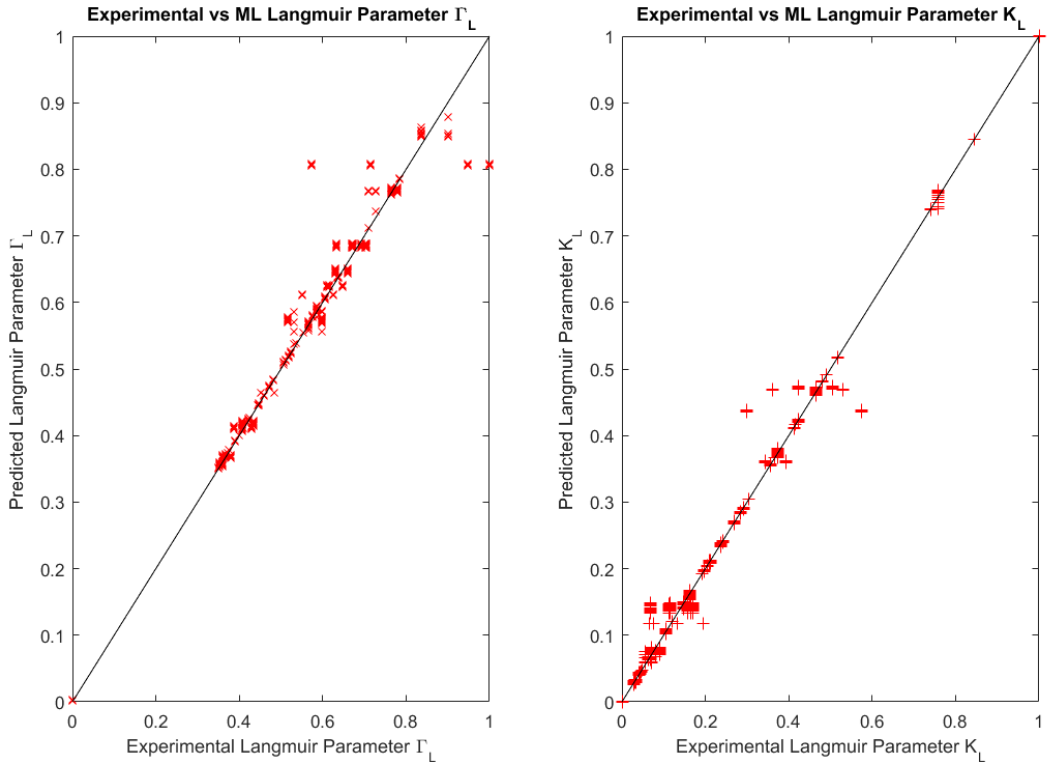

Figure 5.3: Regression Plots for Predicted Langmuir Parameters using Shallow Neural Network

The above figure shows that both neural networks are a good fit for the Langmuir parameters, as a majority of the data fits along the expected fit. However, there are four points, where the model predicts to be 0.8 of the scaled capacity. The corresponding experimental values range between 0.5 and 1.0. This can indicate that the data points have similar inputs that cause the model to estimate 0.8, whereas there are other factors that cause the parameter to change more than expected. A potential method to solve this is to add additional interactions to account for this change. These interactions can either be within the model by increasing the hyperparameters, or by increasing the number of variables in the data set. However, increasing the number of neurons in the shallow layer do not significantly affect the R-value or the pattern observed in these outliers. A similar group of outliers also exist in the second Langmuir parameter K_L at an estimated parameter between 0.4 and 0.5. However, this collection of points varies more compared to the

more consistent group in the first Langmuir parameter. As there is no correlation between the two parameters, these data points are not necessarily the same adsorbent.

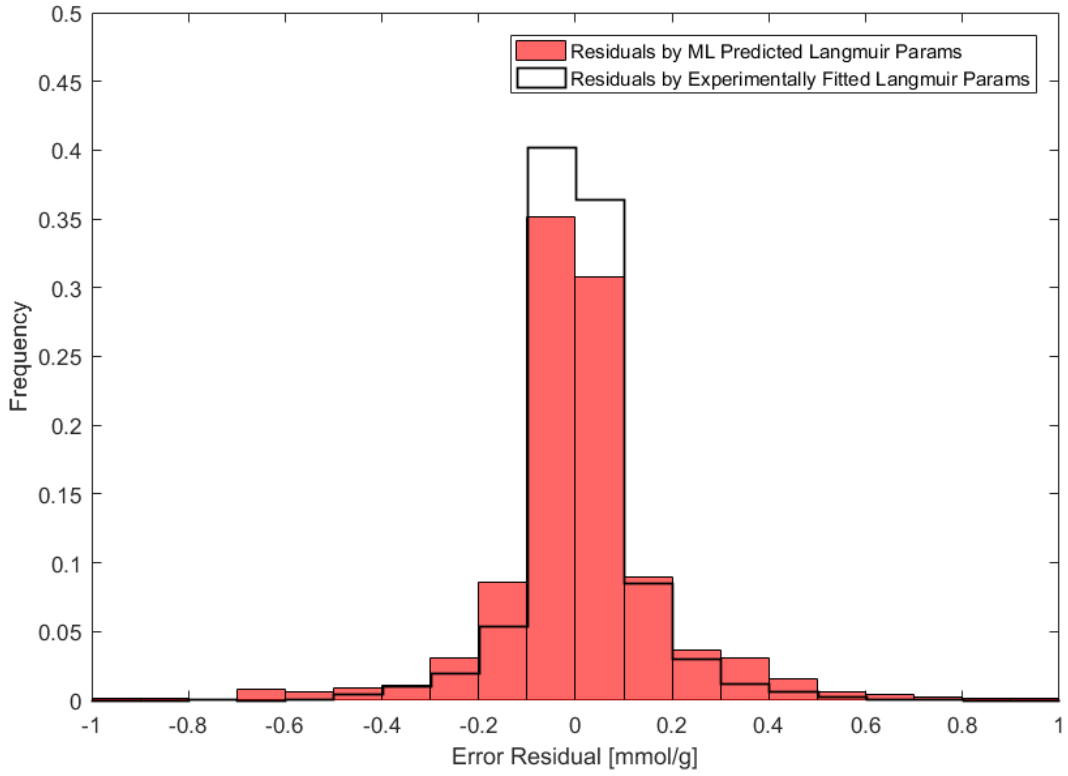

Figure 5.4: Error Histogram for Langmuir Isotherm Shallow Neural Network Model

The above figure shows the adsorption capacity error histogram for the Langmuir isotherm. The red-coloured histogram represents the NN model's output. The unfilled histogram represents the error when using the experimentally fitted Langmuir isotherm parameters, as the experimental parameters also do not represent every data point perfectly. Given that the neural networks are estimating these parameters, additional error is introduced in each model, which is further compounded as each isotherm have multiple parameters. This is seen in the larger variance and less accuracy in the machine learning models compared to the fitted models; the bins closest to the zero error is higher for the fitted parameters, while the bins further away are lower. Using the fitted as a baseline, the machine learning models performance is not poor. The closest bins have a difference of approximately five percentage points for each, which are distributed mostly within a ±0.3 mmol/g error range, with additional outliers outside the range. The machine learning models share a normal distribution pattern with the fitted variables. A table sharing the statistic diagnostics

is shown below. The R-values for the overall dataset and randomly separated data exceed 0.98 for each neural network in the model. The high correlation for all of the models shows similar fitness to the direct prediction.

Table 5.2: R-Values and MSR for Shallow Neural Networks for Langmuir Parameter Prediction

Model	Training R-Value	Validation R-Value	Testing R-Value	Overall R-Value	Overall MSR
Langmuir Parameter $\Gamma_{L\infty}$	0.9808	0.9932	0.9907	0.9832	0.3605
Langmuir Parameter K_L	0.9921	0.9915	0.9929	0.9920	0.0390

The next model, represented by the bottom left plot in Figure 5.1, estimates the Freundlich isotherm, analogously to Langmuir model. The Freundlich isotherm model has two parameters k_F and n_F. The models that estimate k_F and n_F have 12 and 16 neurons in the shallow neural network. The error introduced propagates more due to the reciprocal exponential term n_F. In comparison, the Langmuir parameter K_L propagates error in the denominator which includes a constant unity term. Graphically, the regression points show a greater deviation for a range of points between 0.6 and 0.8 of the scaled experimental capacity. The outlier at approximately 0.9 of the experimental capacity is also further compared to the direct and Langmuir models' regression plots. There is an improvement in accuracy for the group of outlier points above the expected line. While the two other models previously discussed have a constant distance above the line, the outlier shows an improvement in the bulk in the middle of the testing range. There is a loss of accuracy at the more extreme ends. In addition, the model begins to underestimate the bulk of the points over 0.5 scaled capacity. The graphically observed lower accuracy is reflected in a lower overall R-value of 0.9830; while this still indicates that the model fits the data well, there is a noticeable difference between the models.

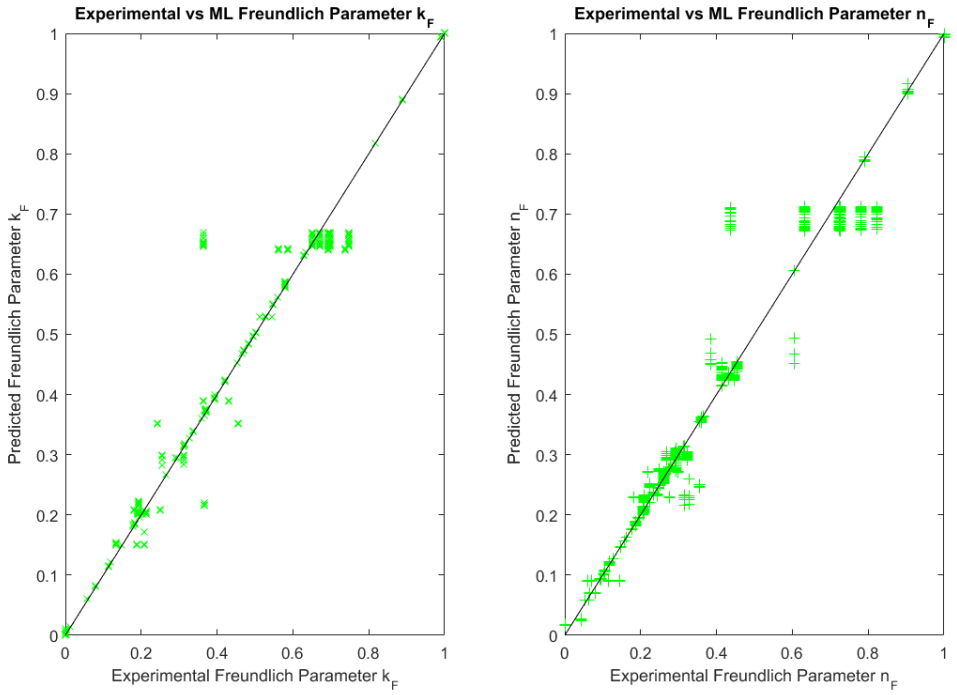

Figure 5.5: Regression Plots for Predicted Freundlich Parameters using Shallow Neural Network

Figure 5.5 above shows the regression plots for the independent Freundlich parameters for each neural network. The majority of the predicted parameters match the experimental parameters. There are a series of that both models predict to be similar. For the parameter k_F there are several conditions that the model estimate to be between 0.65 and 0.70, despite the experimental values ranging the entire part. Similarly, the model for n_F estimates several points between 0.65 and 0.75, which is inaccurate. The inverse exponential n_F affects the regression plot as an overestimation at 0.4 scaled capacity results in the estimate being underestimated. This corresponds to the middle of the regression plot which overall underestimates the points. As the experimental capacity increases, the model tends to overestimate the capacity due to the constant parameter estimate causing an underestimation in the inverse exponent. This error may be due to the model being unable to represent the changing isotherm parameters with the given input; the points do not significantly respond to a change in the process conditions, which can imply an external factor is not represented. If sorbents have similar surface area and pore volumes, then the changing process conditions is not sufficient to estimate the capacity accurately, especially when the model must also represent the other sorbent data points. The error histogram for the adsorption capacity is shown below.

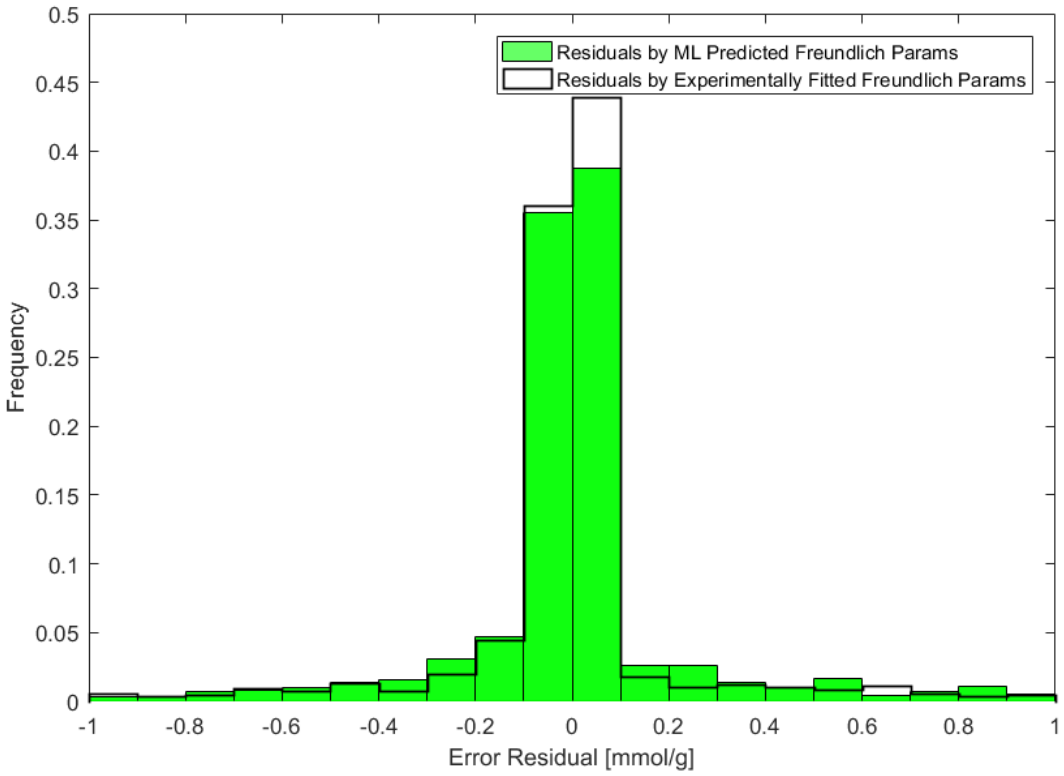

Figure 5.6: Error Histogram for Freundlich Isotherm Shallow Neural Network Model

In Figure 5.6, the error of the overall neural network matches the fitted Freundlich isotherm histogram well for the majority of the points. However, there is a significant deviation for the bin encompassing the 0.0 to 0.1 mmol/g error in the comparison. There is approximately five percentage point difference between the experimentally fitted isotherm and the model. Instead, these errors are distributed in different bins for residuals over ±0.1 mmol/g. Part of the error is previously discussed in the cluster of points visible in the individual parameter regression plots. This corresponds to the positive error residuals bins' increases; this is supported by the increase only significantly occurring in three discontinuous bins. From Figure 5.5, the cluster of points are cleanly divided into groups of points aligned with the experimental values; this is an artifact of the data collection, where the points provided of this sorbent are reported at similar conditions for similar capacities. As such, the groups of errors are then appropriately reflected in the error histogram. Outside of these clusters, the bins at ±0.1 to ±0.2 mmol/g are also greater due to the error propagated in the models; this is similar to the error seen in the Langmuir model. The R-values for the different parameters for each group is presented below. Despite the outliers, the R-

values show a good fitness for the model. This is due to the number of outliers being low compared to the majority of the data. The R-value thus indicates the model works whereas the deviations that occur are significant.

Table 5.3: R-Values and MSR for Shallow Neural Networks for Freundlich Parameter Prediction

Model	Training R-Value	Validation R-Value	Testing R-Value	Overall R-Value	Overall MSR
Freundlich Parameter k_F	0.9885	0.9902	0.9873	0.9887	0.0414
Freundlich Parameter n_F	0.9846	0.9754	0.9903	0.9838	0.0194

The third model represented in the lower right corner in Figure 5.1 is the combined Langmuir-Freundlich model. By encompassing both the exponential and divisor terms in the parameters, the performance for the ideal Langmuir-Freundlich model can represent adsorbents that work for either individual Langmuir or Freundlich isotherm. However, the error propagation becomes more severe with the addition of a third parameter term; this corresponds to a third machine learning model and its corresponding error. From the regression plot, this is apparent with the distinct isotherms that are not accurately represented at the lower capacities; these linear points that appear are obvious indications that the model is not accurate in the lower range. Additionally, the outlier isotherm described in the direct and Langmuir isotherm models is again visually apparent; this indicates that the strength of the combined isotherm does not appear in this model whereas the weakness with the error is exacerbated. The overall R-value for this isotherm is 0.9701. While this still describes a good fit, this is lower than the three previous models.

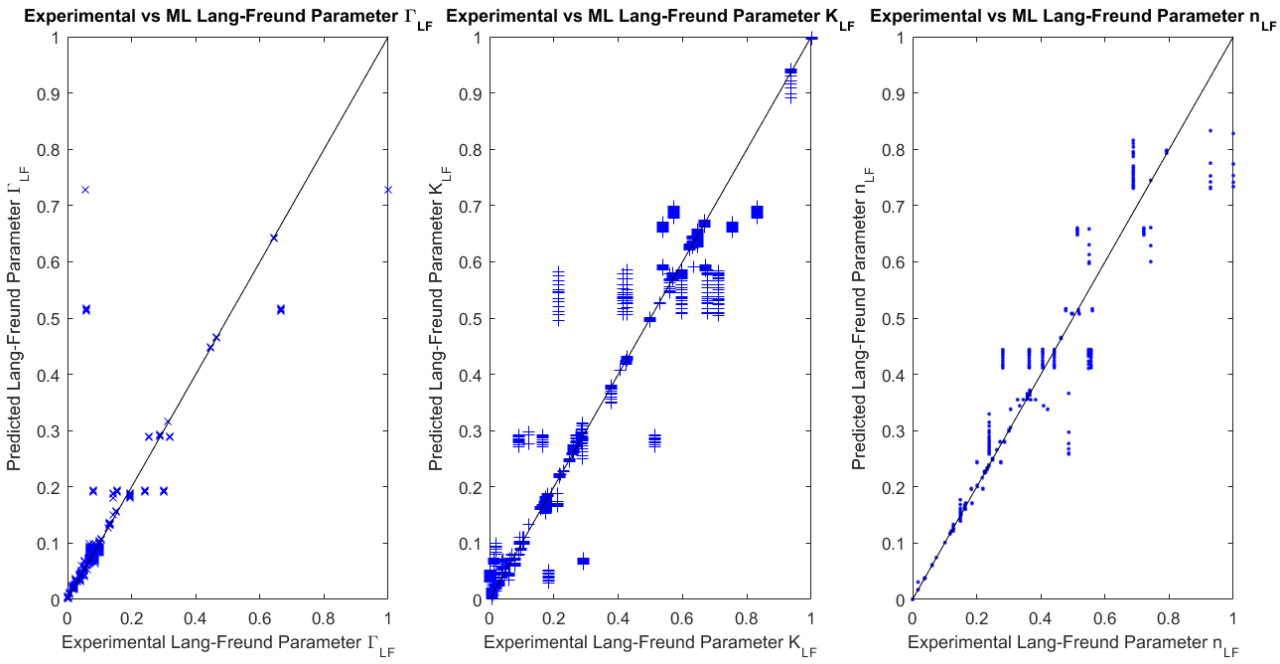

Figure 5.7: Regression Plots for Predicted Langmuir-Freundlich Parameters using Shallow Neural Network

From the above figure, all three neural network models show inaccuracies, explaining the lower overall R-value. For the Γ_{LF} model, the majority of the points are located on the regression line from 0.0 to 0.1 capacity. This indicates that the parameters are not evenly spread throughout the range, which is not ideal for modelling. However, there are distinct outliers where the model grossly overestimates the Γ_{LF} parameters. Experimentally, the parameter is found to be 0.1 whereas the ML model estimates the parameter to be approximately 0.51 or 0.73. The Γ_{LF} parameter acts as a factor for the remainder of the isotherm which causes the adsorption capacity to be overestimated. This corresponds to the outliers forming a linear pattern above the regression line in Figure 5.1; these adsorption capacities are multiplied by a higher factor which is revealed by the steeper slope in the regression plot. These outliers remain in spite of increasing the neuron count or when the input dataset is randomly re-partitioned between training, validation, and testing groups. Additionally, there are a series of points estimated at 0.2 capacity whereas the experimental values vary between 0.1 to 0.35. These points are similar to the previously seen pattern in the Langmuir and Freundlich isotherm models. The pattern of horizontally aligned points appears in the regression plots for the two other isotherm parameters. Aside from these outliers, the remainder of the points for Γ_{LF} match the experimentally fitted values. These outliers have large enough errors

to largely reduce the overall R-value to 0.9014, which is significantly lower than the previous isotherm parameters' correlation. For the parameter K_{LF}, there are outliers that occur throughout the capacity range. The horizontal aligned outliers are present, but the remainder of the outliers do not share a pattern. The R-value for this neural network is 0.9681 which is also lower than the parameters in the previous models. The third parameter n_{LF} shares the horizontal pattern but also has distinctive vertical patterns as well. While this pattern is less significant for other parameters, the height of the vertical pattern is more severe.

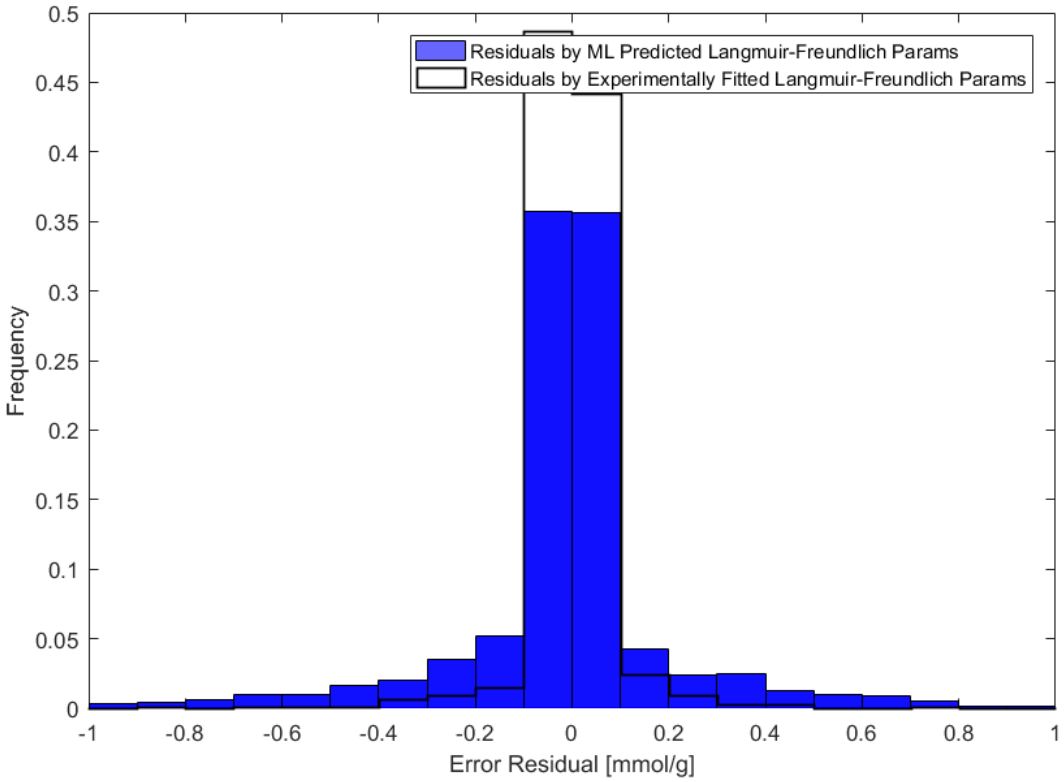

Figure 5.8: Error Histogram for Langmuir-Freundlich Isotherm Shallow Neural Network Model

The error histogram for the Langmuir-Freundlich models shows the greater error introduced through the additional parameters and lower model accuracy. The two bins closest to the zero-error total approximately 71.4% of the residuals. In comparison, the equivalent bins for the direct, Langmuir and Freundlich ML models total 56.7%, 65.9% and 74.3% respectively. The Langmuir-Freundlich model does well for these closest bins. However, the four most extreme bins for either side are large, indicating there are slightly more data points that have greater error; this difference does not exceed one percentage point and are not statistically significant. However, given the lower

R-value, the model represents the bulk of the data points accurately but has larger errors for outliers in comparison to the other models. The model also pales in performance to experimentally fitted parameters. The residual distribution for the fitted distribution is less wide; the seven most-extreme bins on one end total less than one percent total.

Table 5.4: R-Values and MSR for Neural Networks for Langmuir-Freundlich Parameter Prediction

Model	Training R-Value	Validation R-Value	Testing R-Value	Overall R-Value	Overall MSR
Langmuir-Freundlich Parameter $\Gamma_{LF\infty}$	0.8969	0.9143	0.9815	0.9014	32.7956
Langmuir-Freundlich Parameter K_{LF}	0.9700	0.9612	0.9573	0.9681	0.0077
Langmuir-Freundlich Parameter n_{LF}	0.9771	0.9776	0.9840	0.9775	0.0020

The above table exhibits the lower R-values calculated from the three neural networks relative to the previously prepared networks. As previously mentioned, the model for Γ_{LF} shows a notable decrease to 0.9014 whereas the two other models' R-values still remains above 0.95. The MSR for this parameter is also notably higher due to the large residual in the outliers; while the MSR is not scaled, the equivalent coefficients determined in the Langmuir and Freundlich models have a much lower MSR in magnitude. All of these indicate that the Langmuir-Freundlich does not have higher correlation than the other direct and isotherm adsorption capacity models. The Langmuir-Freundlich isotherm show better performance for adsorbents in general when fitted experimentally; however, the total of three models and the distribution of the parameters makes it more inaccurate overall for machine learning. The greater performance in experimental fitting is not sufficient compared to the inaccuracies gained with the additional model.

A summary of the initial iteration of the shallow neural networks is shown below. Combined with the regression plots, the direct prediction and the Langmuir models have the highest R-values with 0.9901 and 0.9906, respectively. The Freundlich model has a lower R-value at 0.9830, while the combined isotherm has the lowest R-value of 0.9701. The number of neurons is chosen after several runs, after which increasing does not affect the accuracy of the model.

Table 5.5: Summary of Individual & Combined Shallow Neural Networks Models

Model	Number of Hidden Layers	Number of Neurons	Overall R-Value	Overall MSR
Direct Prediction Model	1	20	0.9901	0.0768
Langmuir Isotherm Model	-	-	0.9906	0.0725
Langmuir Parameter $\Gamma_{L\infty}$	1	14	0.9832	0.3605
Langmuir Parameter K_L	1	14	0.9920	0.0390
Freundlich Isotherm Model	-	-	0.9830	0.1311
Freundlich Parameter k_F	1	12	0.9887	0.0414
Freundlich Parameter n_F	1	16	0.9838	0.0194
Langmuir-Freundlich Isotherm Model	-	-	0.9701	0.2293
Langmuir-Freundlich Parameter $\Gamma_{LF\infty}$	1	18	0.9014	32.7956
Langmuir-Freundlich Parameter K_{LF}	1	12	0.9681	0.0077
Langmuir-Freundlich Parameter n_{LF}	1	12	0.9775	0.0020

From these initial results, the direct prediction and the Langmuir isotherm perform well. However, the two other models show more notable patterns in the regression plot, indicating that there can be improvements made to this. Thus, the next iteration changes the hyperparameters and introduces new variables to better capture the interactions. First, the number of layers is increased to two, to increase the interactions between neurons; the number of neurons in each layer is lowered to avoid overfitting, despite the risk being low due to the relatively large number of data points. As well, the category of adsorbent and the two Langmuir parameter estimates are used as variables for the new networks. The dataset categorizes the adsorbents into four main categories: carbon-based, MOF, POP, and zeolites. As per the previous section, additional categories exist for the adsorbents but are not represented in the filtered data set. To account for the categorical nature, the input is fed as an array of four elements; each element corresponds to a category. If the category matches the adsorbent, one is entered in the array and zero otherwise. The breakdown of the number of adsorbents in the filtered data set is presented in the table below. The appearance of one zeolite significantly affects the model when predicting for zeolite compounds. As well, the considerable number of data points stem from a limited number of sorbents.

Table 5.6: Adsorbents Separated by Category

	Entire Data Set	Category 1 Carbon-Based	Category 4 MOF	Category 5 POP	Category 7 Zeolite
Number of Unique Adsorbents	25	8	10	6	1
Number of Data Points	2125	1130	636	313	46

As described in the Literature Review, the Langmuir parameter Γ_L and K_L represent the maximum adsorption capacity and the adsorption equilibrium constant, respectively. These parameters can be used as inputs for the model; this is also useful given the high accuracy in the Langmuir isotherm neural networks and the prevalence of the Langmuir isotherm. Including the Langmuir parameters as variables are only viable for the Freundlich and combined Langmuir-Freundlich models. The Freundlich and Langmuir-Freundlich parameters do not have obvious relationships to the Langmuir parameters; more accurately, the parameters depend on the maximum capacity and the equilibrium constant for the adsorption process, but the exact relationship is not known. In contrast, the relationship between the capacity and the Langmuir parameters as variables is known from the isotherm equation; machine learning can identify the isotherm implicitly which is not conducive to the objective of the model. More directly, a model that predicts the Langmuir parameters cannot have inputs that are identical to the outputs. This indicates that the Langmuir parameters should function as inputs only for the Freundlich and Langmuir-Freundlich models. The Langmuir parameters inputs are based on the parameters estimated from the Langmuir parameter model. In practical usage, the Langmuir isotherm may not be known, so using the model to further estimate it may be required. It is also noted that, for an adequately sized perfect neural network, the relationship in the Langmuir model would be implicitly included in the other models.

When implementing these changes, the R-value is used as a preliminary indicator for the correlation to the target. The data set are randomly selected and distributed between the training, validation, and testing datasets, as previously done. Applying this random selection results in equivalent R-values between the two-values. To investigate the effect of these new parameters, the previous training, validation, and testing data distribution is reused for the models with the additional parameters. The regression plots for the new models are shown here.

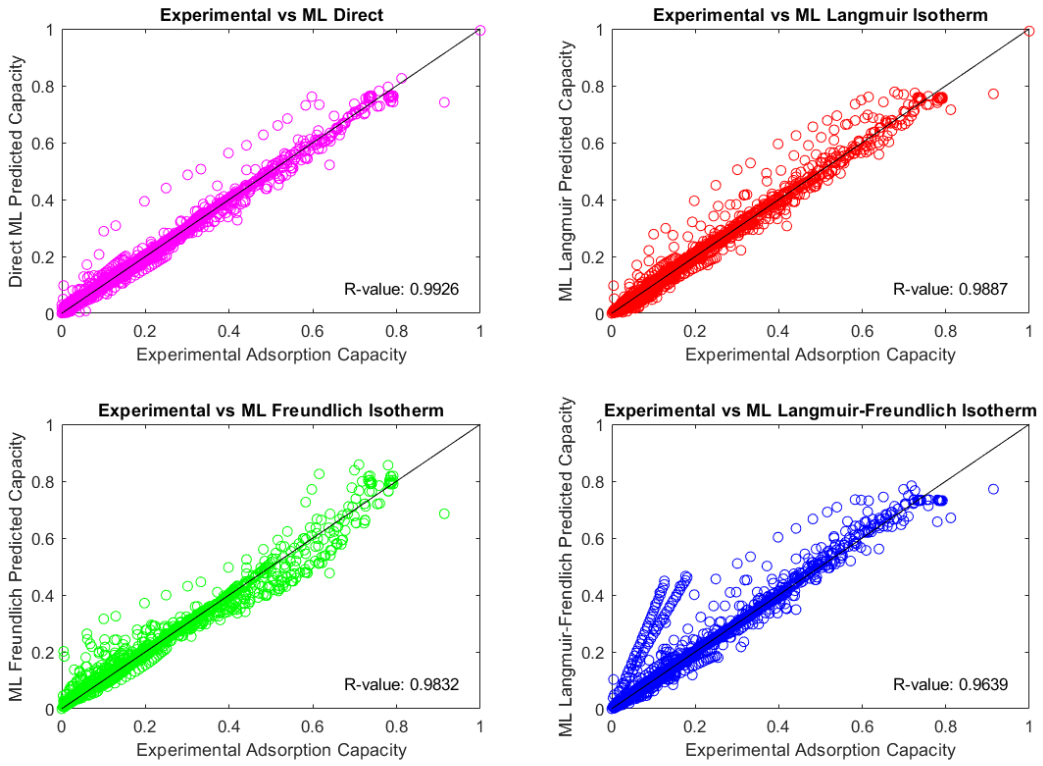

Figure 5.9: Regression Plots for Adsorption Capacity Models with Additional Inputs & 2 Hidden Layers using Neural Networks

The above Figure 5.9 exhibits identical patterns to the previously described Figure 5.1. The collection of outlier points above the four models, the visually subjective curve in the Freundlich model and the two collections of outlier isotherms in the combined Langmuir-Freundlich model remain in the new figure. However, the R-values for all of the models, except the Langmuir model, is slightly greater; the R-value difference, however, may be small enough to be non-significant when comparing the models. This is also supported by the similar R-values when training the model on randomly distributed data sets. Below is a collection of error histograms for the completed model. The histograms describe a similar trend to the original neural networks, with the majority of the points gathered around the zero error and the machine learning programs having less accuracy for the fitted parameters.

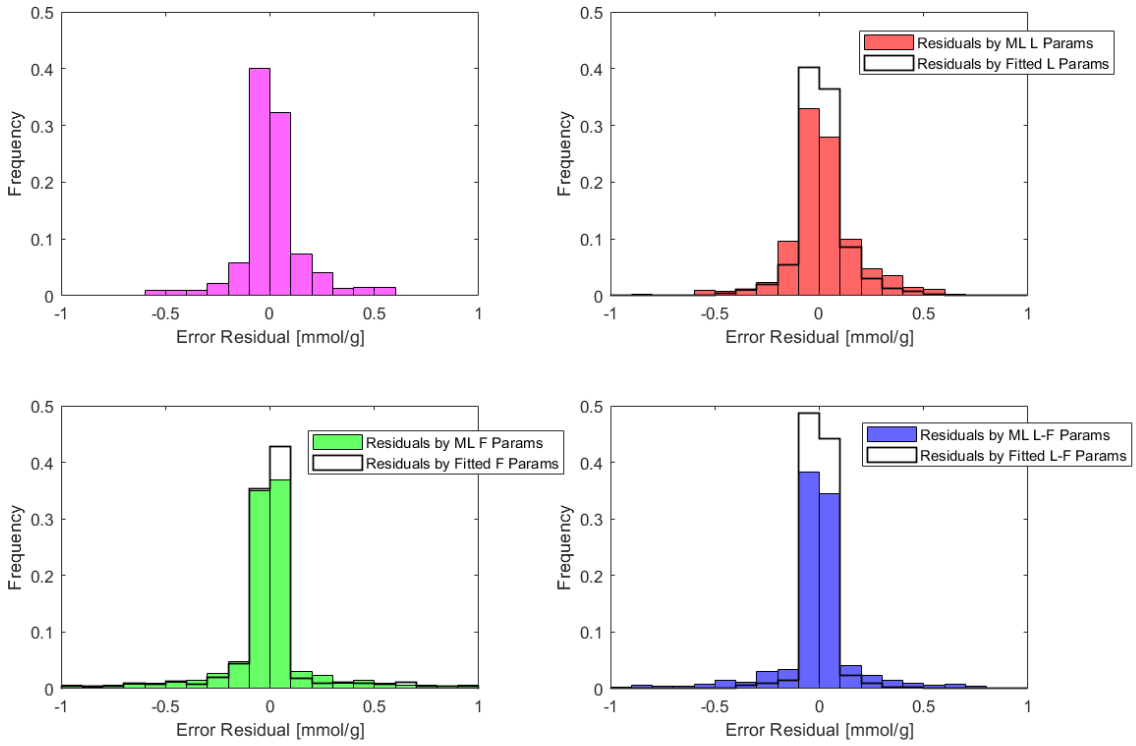

Figure 5.10: Error Histograms for Adjusted Neural Network Models

Comparing the original and adjusted neural networks, the new adjustments do not significantly impact the model response. The trends described in the original model are still apparent in the adjusted model. As well, there are the R-value do not significantly change between the adjusted models. The higher R-values for the direct and Langmuir model are not significantly higher; instead, the improvement cannot be separated from the variance from the randomized partitioning for training and testing data. The error histograms for the adjusted model similarly do not have explicit trends but are lower than the fitted parameters, as expected.

More complex machine learning programs can provide different models that may have different strengths. MATLAB provides several built-in ML functions. In addition, the theoretical improvements in adjusting the models do not realize any improvements in the response. The models are trained with the original data set, where the adsorbent category and the additional Langmuir parameter is not trained; as the additional adjustments do not change the response significantly, the model is kept simpler.

The machine learning models trained are an ensemble model, a GAM model, a GPR model and an SVM model. The regression plots are shown below, and the error histograms are shown in the appendix.

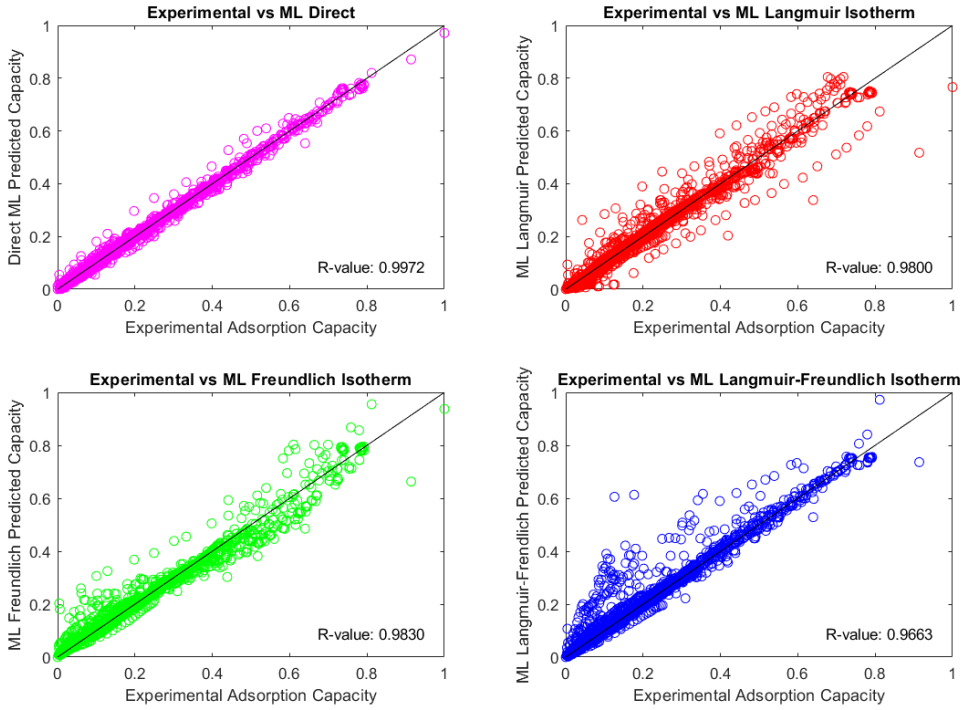

Figure 5.11: Regression Plots for Regression Ensemble ML Models

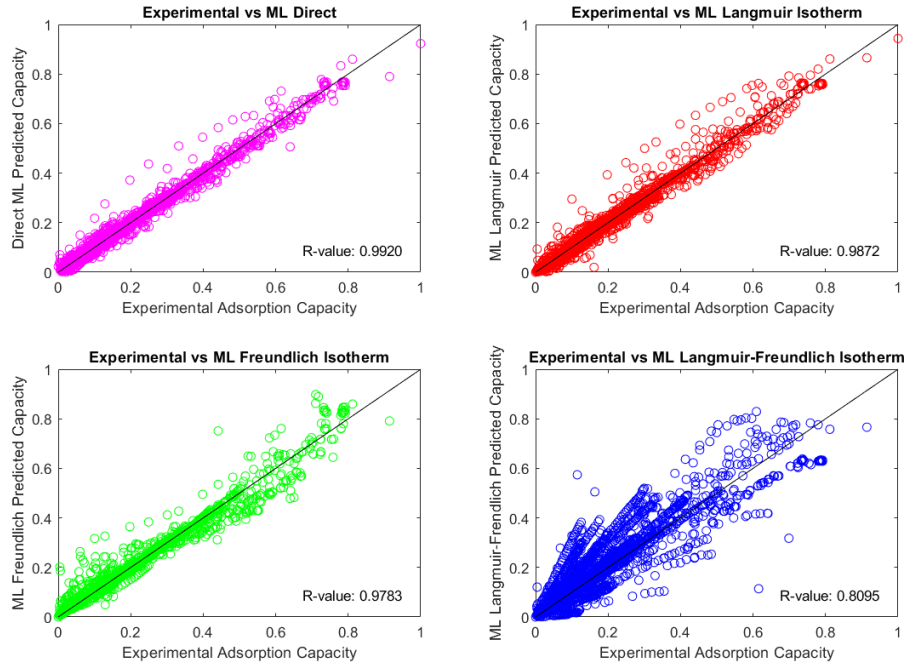

Figure 5.12: Regression Plots for GAM Models

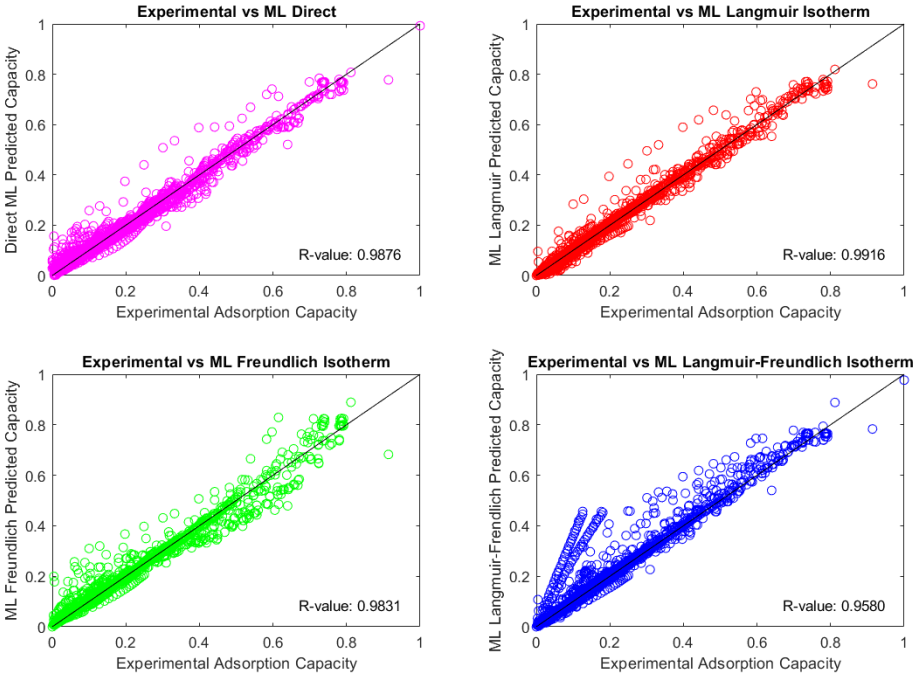

Figure 5.13: Regression Plots for GPR Models

For the three types of ML models ensemble, GAM and GPR, estimating the adsorption capacity directly and through the targeted isotherm parameters show a high amount of fitting. The direct capacity and the Langmuir isotherm both show a high degree of correlation within the data set with R-values above 0.96 regardless of the ML algorithm. The ensemble model exhibits a lower amount of correlation relative to the other models, which is graphically observed in the greater dispersion of points under the target line. The GPR model shows a slightly higher R-value for the estimates from the Langmuir isotherm, which is not typical for the other models; however, the difference is negligible for not significant with both the direct and Langmuir-estimated models achieving above or equal to 0.98 for the R-value. The Freundlich isotherm model shows slightly worse performance, consistently for the three models. All three Freundlich models do not perform as well at the higher adsorption capacities, where the model tends to increase greater than the experimental value. This can be seen in the Freundlich isotherm itself, where the exponential term can exacerbate errors outside of the given range. The Langmuir-Freundlich isotherm has the lowest correlation, with immediately visual artefacts visible in the above figures. The ensemble and GPR model show a good correlation above 0.95. The overall collection of data fit the experimental data well, while most of the outliers remain above the fitted line. This may indicate the model is overestimating the points; most notably, there are lines of points that increase at a greater linear rate above the normal line. This can be attributed to a higher multiplier to the isotherm, as estimated by the individual model estimating the first Langmuir-Freundlich parameter. However, the same trend is not described by the model trained using GAM. The Langmuir-Freundlich model generated by GAM shows significant issues in performance, with a low R-value of 0.8095. The model shows difficulty in estimating the different adsorbents' performances, as seen in the different linear collection of points both above and below the normal line. While this indicates a potential issue with the parameter $\Gamma_{LF\infty}$, a smaller density of points is concentrated close to the regression line. Instead, they are distributed above the regression, resulting in greater residuals and a lower overall correlation in the GAM model.

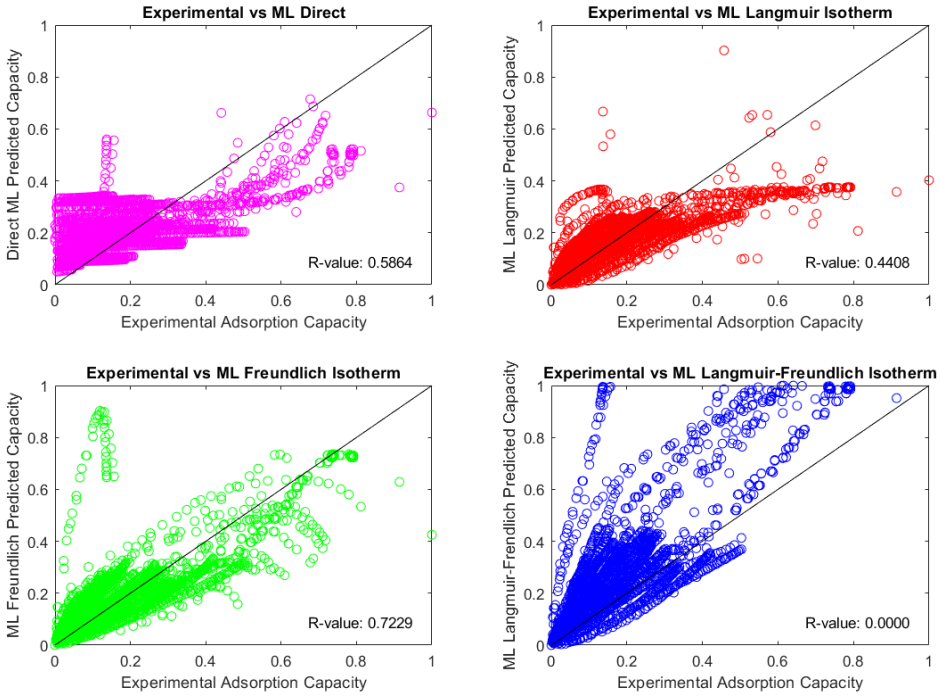

Figure 5.14: Regression Plots for SVM Models

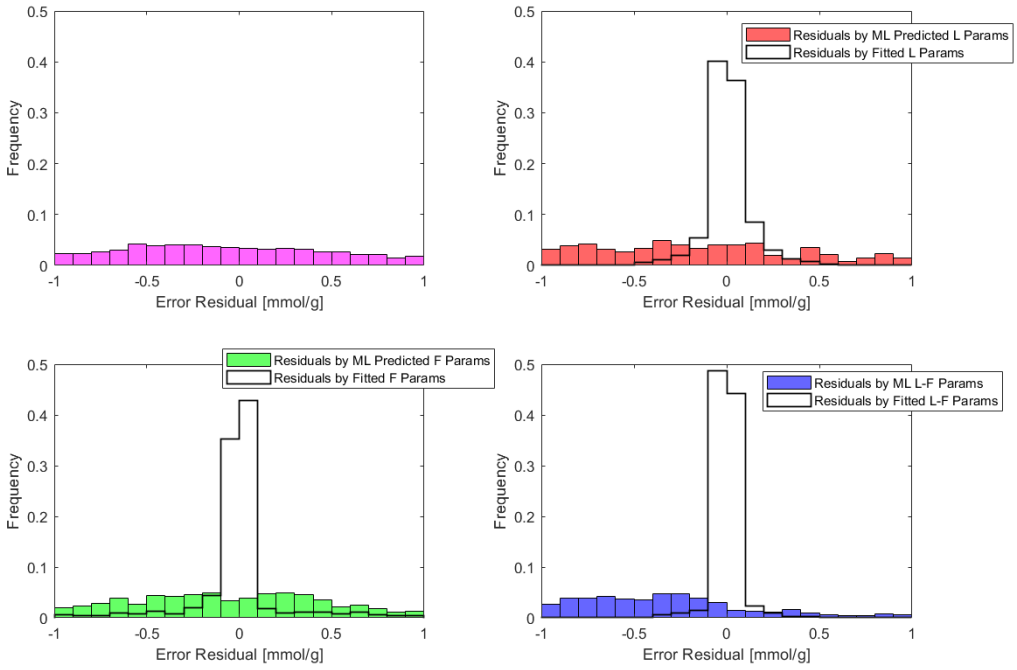

Figure 5.15: Error Histogram for SVM models

The SVM model has the poorest performance, which is immediately visible in the figure above. The direct adsorption capacity, which performs the best among the other machine learning programs, shows poor performance. The error histogram for the direct prediction also does not exhibit the expected normal distribution of the residuals. Instead, the frequency in each bin is approximately equivalent to each other. This is an indication the model does not estimate the target response well; instead, this error histogram indicates that the model is almost random, which is not expected. The other models do not perform as well as the others, indicating that using SVM for regression in this context is not valid. The margin may be too lenient which is not sufficient in any reasonable estimation from the model.

An adsorbent separate from the training data is chosen to independently examine the model's responses. The adsorbent in question is MOF-14 or $[Cu_3(BTB)_2(H2O)_3]\cdot(DMF)_9(H2O)_2$. Originally described by Chen *et al*. [27], the adsorption data is gathered from Karra *et al.*'s work, as gathered in NIST's adsorption database [28]. In addition, Karra *et al*. also provides the relevant adsorbent parameters; the BET surface area and pore volume are reported as 1398 m^2/g and 0.57 cm^3/g. The figures below show the regression plot on top of the adsorption curve, for the various models. A table is also presented showing the R-values for each model.

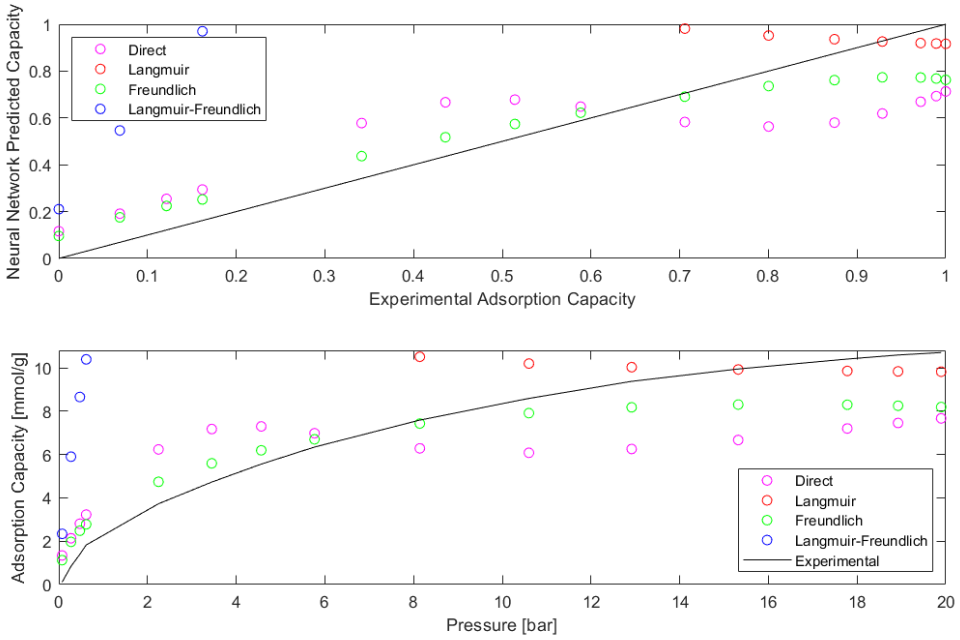

Figure 5.16: Neural Network Model Response to Validation Data

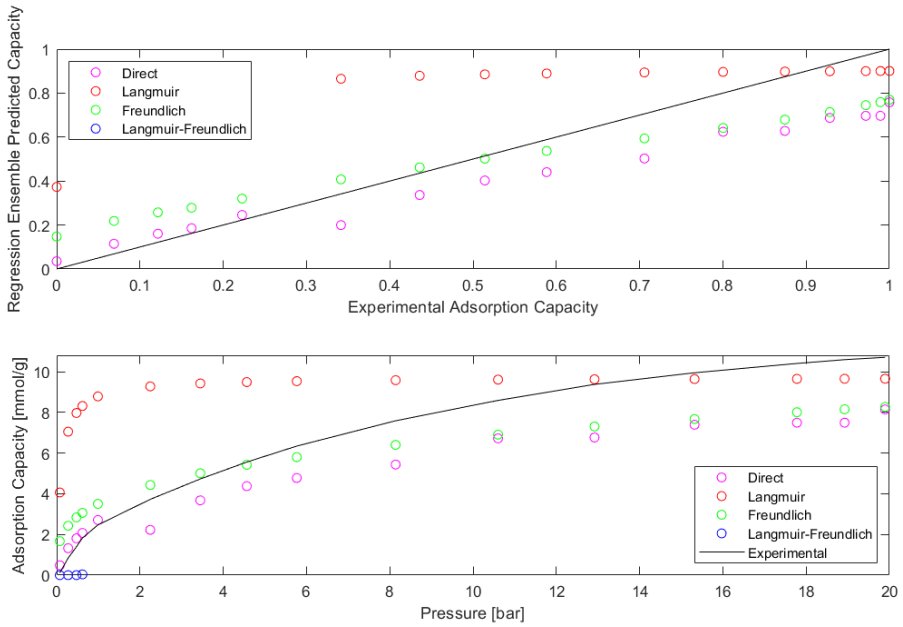

Figure 5.17: Regression Ensemble Model Response to Validation Data

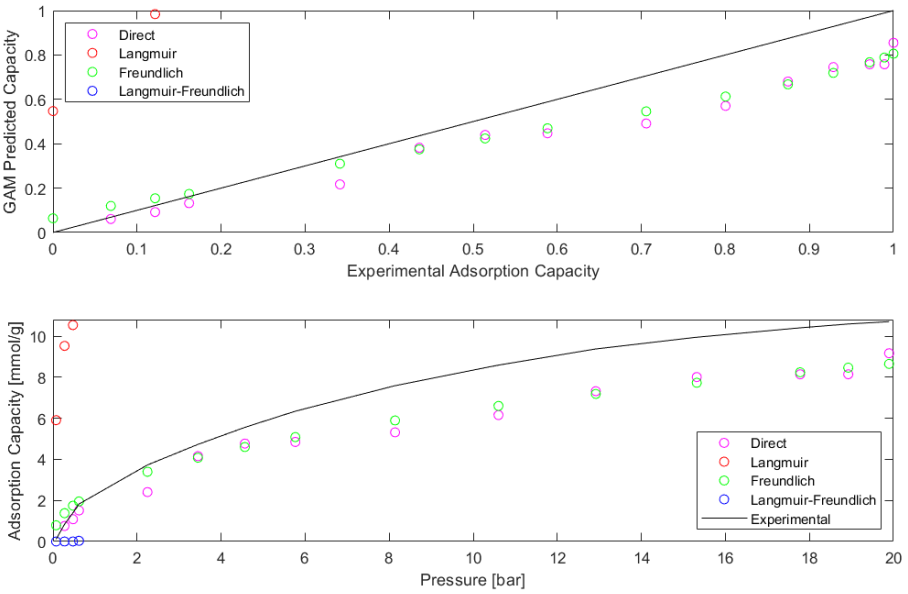

Figure 5.18: GAM Model Response to Validation Data

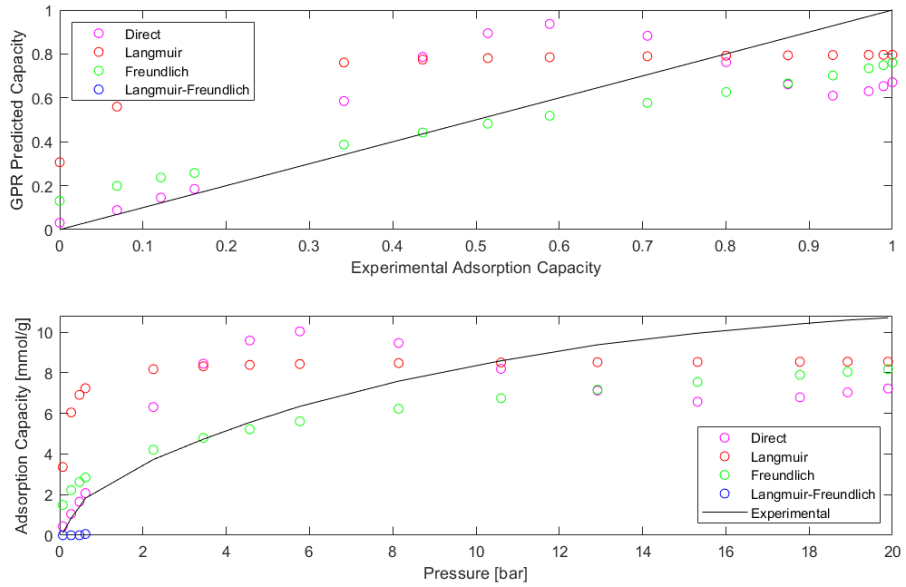

Figure 5.19: GPR Model Response to Validation Data

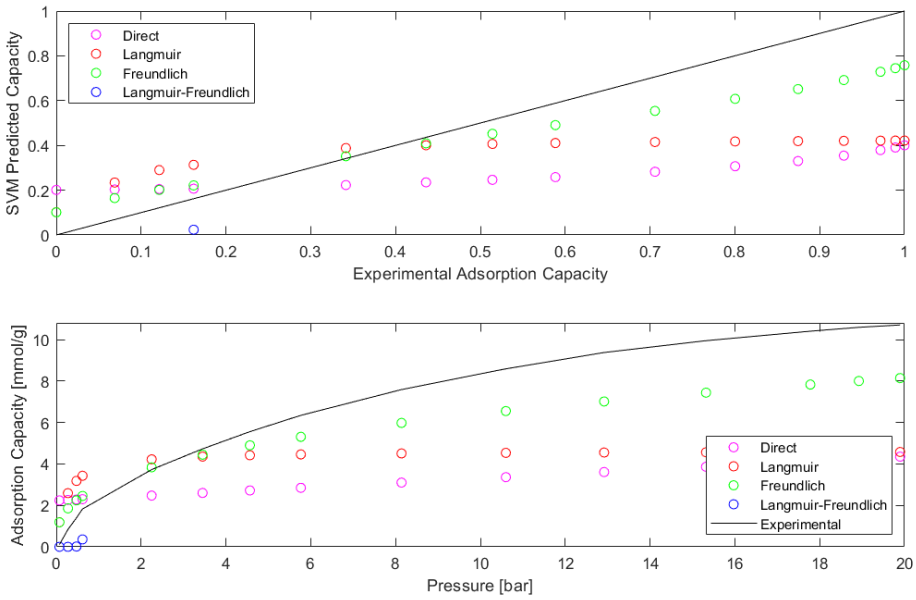

Figure 5.20: SVM Model Response to Validation Data

Table 5.7: R-Value for Estimated Response for MOF-14 Sorbent

	Direct Prediction	Langmuir	Freundlich	Langmuir-Freundlich
Neural Network	0.7795	-	0.9305	-
Regression Ensemble	0.8589	-	0.8954	-
GAM	0.9028	-	0.9139	-
GPR	0.6868	0.4804	0.8911	-
SVM	-	0.1482	0.8882	-

From the above figures and tables, the models have significant difficulties in estimating the adsorption capacity outside of the training data. The blank spots in Table 5.7 indicate that the calculation for R-value returns an imaginary number, and the error in the model cannot be reasonably explained by any error from regression. This is reflected in the model response, which are significantly different from the normal line. The Langmuir-Freundlich models increase faster than the experimental findings and do not appear in the figures. Likewise, the Langmuir model also exhibits this behaviour for the neural network model, unexpectedly. Furthermore, the Freundlich isotherm shows the greatest performance; the two performance is superior to the direct prediction capacity, which is comprised of only one separate model.

The Aspen Adsorption model previously prepared can also be used to examine the model responses. Running the model under the same conditions with different isotherm parameters allow quantitative performance comparisons between the models. The breakthrough curves are shown below. In addition, the amount of product produced and the combined cycle time for two cycles is accounted for. A table below is presented to show the Freundlich parameters used.

Table 5.8: Estimated Freundlich Parameters for MOF-14 at Ambient Conditions

	Experimentally Fitted	Neural Network	Regression Ensemble	GAM	GPR	SVM
Freundlich Parameter 1	2.539	6.036	1.536	1.909	2.469	-708.383
Freundlich Parameter 2	2.016	4.932	1.990	1.768	2.740	-119.174

The table immediately illustrates the difficulty in using the SVM model. The negative Freundlich parameter 1 acts as a negative coefficient, which renders the capacity as negative. Unfortunately, the SVM model cannot be used in the Aspen Adsorption as a result; given the poor performance even within the trained data, the SVM model should not be used in this context. While the optimization is set in MATLAB, it is evident that SVMs do not predict the target response with the given data set. The other models respond relatively well with the given data set; as such, it is concluded that SVMs do not suit this particular data set. The optimization of the margin hyperparameter may be too lenient, allowing a large margin to fit the data; the trends discussed from the figures of neural networks may perform poorly with the margin approach that regression SVMs use.

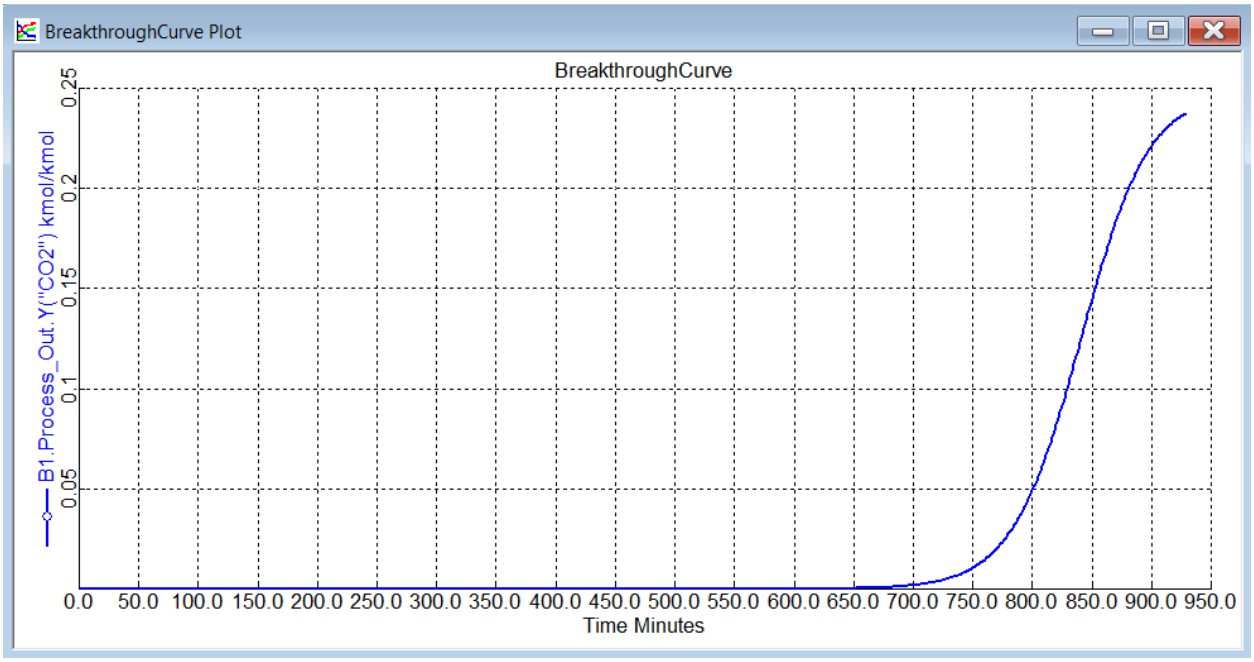

Figure 5.21: Breakthrough Curve for Aspen Adsorption Simulation using Fitted Parameters

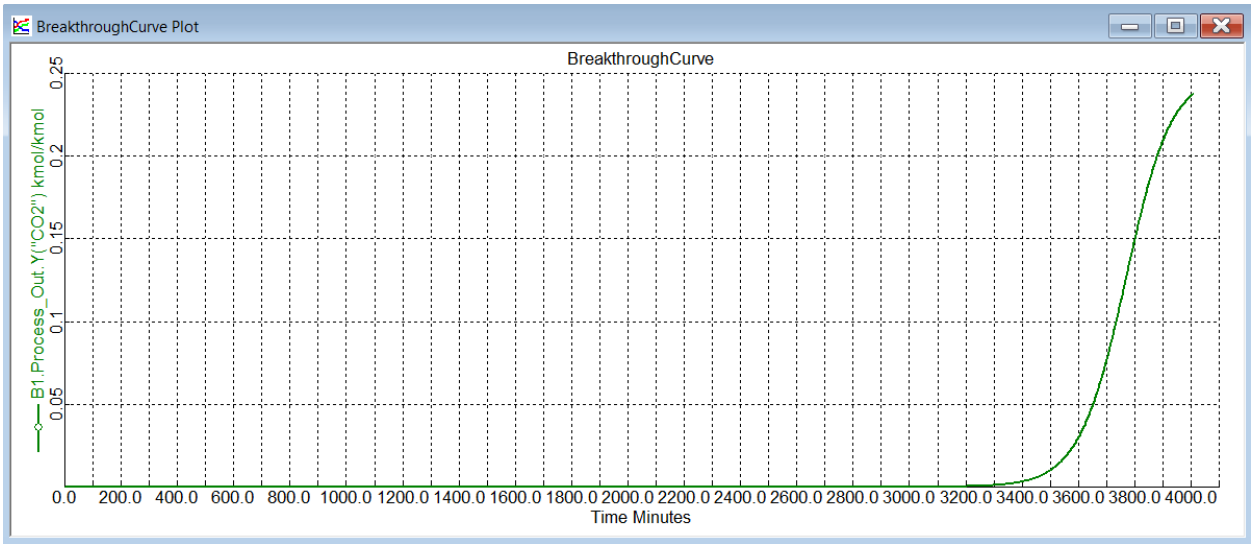

Figure 5.22: Breakthrough Curve for Aspen Adsorption Simulation using Neural Network Estimated Parameters

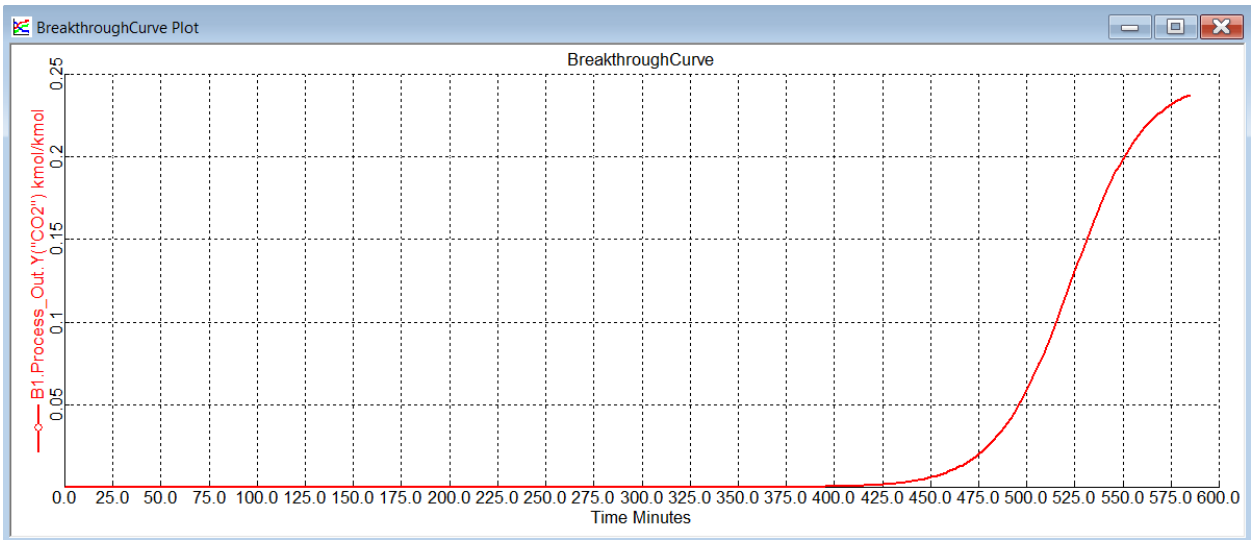

Figure 5.23: Breakthrough Curve for Aspen Adsorption Simulation using Regression Ensemble Estimated Parameters

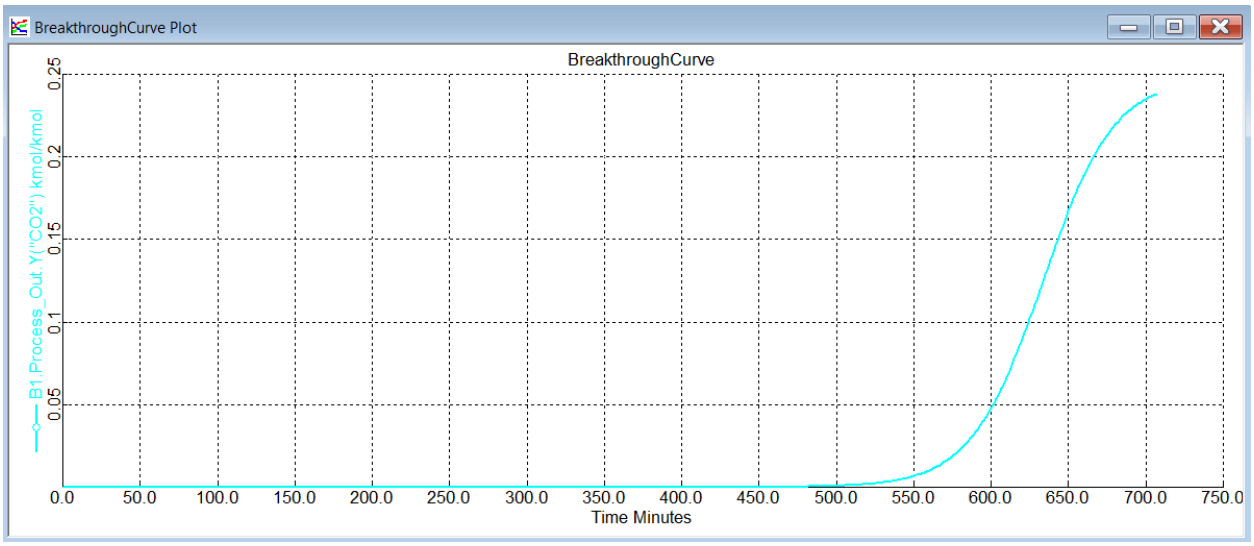

Figure 5.24: Breakthrough Curve for Aspen Adsorption Simulation using GAM Estimated Parameters

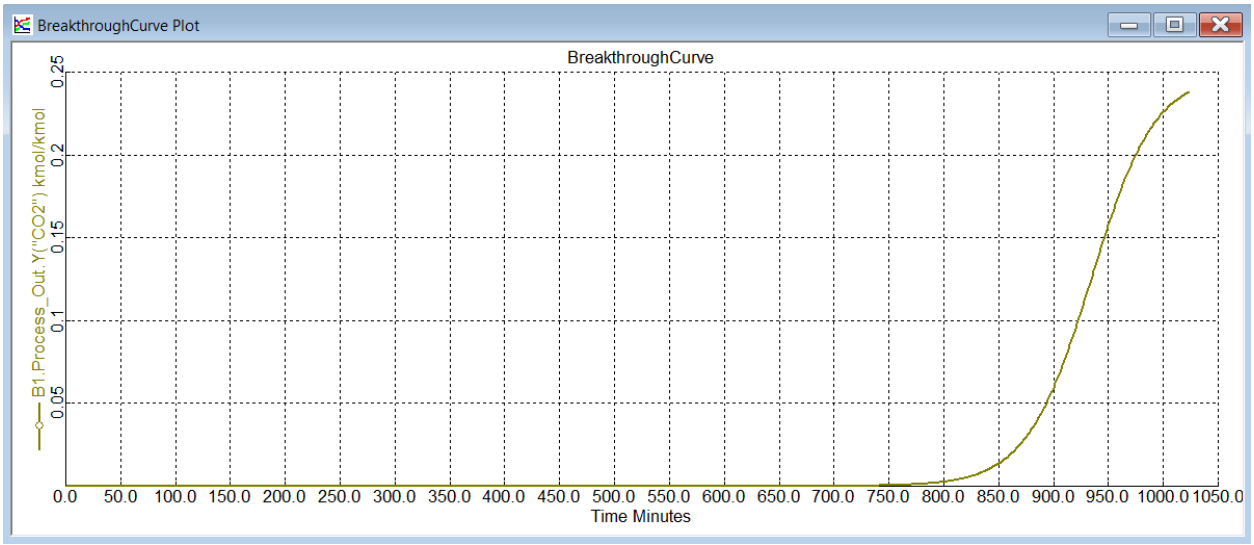

Figure 5.25: Breakthrough Curve for GPR Models

Table 5.9: Aspen Adsorption Response to ML Models' Output

Model	Breakthrough Time [min]	CO_2 Recovered [mol]	Two Cycle Time [min]
Fitted Parameter	928.33	13.97	5410
Neural Network	4008.33	62.41	25376.67
Regression Ensemble	585	8.63	3456.67
GAM	710	7.48	3456.67
GPR	1023.33	24.63	9526.67

From the table above, the fitted parameter from the NIST adsorption database shows that the breakthrough time is expected to be 928.33 min. The GPR model is the closest at 1023.33 min, which results in a 10.6% difference. The 100-minute difference is relatively large to the fitted breakthrough time; however, the other models show much larger difference. The regression ensemble and GAM models have a much lower breakthrough time at 585 min and 710 min, respectively. This is reflected in the smaller amount of CO_2 recovered in two cycles and the shorter cycle times. This is reflected in the lower isotherm coefficient, where the ensemble model and GAM model have parameters of 1.54 and 1.91, respectively. The fitted model has a parameter of 2.539; GPR has a close approximation of 2.469, within 3% of the fitted value. The neural network also exhibits a great overestimation in both the carbon dioxide recovered and the cycle and breakthrough times. The Freundlich parameters are both overestimated by over 100%. The overall response for MOF-14 is not as extreme, as observed from Figure 5.16; regardless, the combined neural networks perform considerably poorer than the other models.

Finally, the cycle times and carbon dioxide recovery amount can be used to estimate the average CO_2 recovery flow rate. Given that the first cycle starts from an initial state, the cyclical steady state values for the average flow rate is not recorded; as more cycles are run, the flow rate should equilibrate at a certain amount. The flow rates between the models are relatively close, despite the differences in times and molar amounts. The neural network, ensemble and GPR are all within 5% of the 2.58 kmol/min product recovery. From a preliminary design perspective, the models can estimate steady state flow with a reasonable amount of accuracy. However, the error shown previously makes it impossible to assume this is true for other adsorbents. While the machine learning models are unable to connect the capacity and the adsorbent, the work shows the capabilities of the models. Despite the different array of models used for training, most of the

models show good performance; generalizing the model has difficulties, which may be associated with the more specific parameters of the sorbents that are unavailable. Characterizing the adsorbent with a larger, more robust data set is necessary to fulfill the original model objective.

Table 5.10: Averaged CO_2 Recovery Rate for Each Model

Model	Averaged CO_2 Recovery Flow Rate [kmol/min]
Fitted Parameters	2.58
Neural Network	2.46
Regression Ensemble	2.50
GAM	2.16
GPR	2.59

Chapter 6: Conclusion & Future Work

The models show the possibility of machine learning in the scope of carbon capture with adsorption. As the collection of adsorbents grows larger with each novel development, so does the need to collect the details of the adsorbents. This is attempted in Chapter 2, where summary papers are used to identify adsorbents for carbon capture. While gathering this information, it is apparent that the information is not consistently available. However, textural properties such as surface area and pore volume, combined with NIST's adsorption database providing process conditions, sorbent capacities and fitted isotherm parameters, can create a set of 2,125 data points, spanning twenty-five adsorbents.

The process of creating an adsorption bed model is also examined; while there are difficulties in preparing a suitable model, a model is created in Aspen Adsorption. The use of ML methods is examined in Chapter 4. A preliminary model is created with neural networks which shows a high level of correlation, with R-values above 0.95 for the four models created. A potential improvement is proposed to increase the number of adsorbent variables, where the result does not show a marked improvement. As such, the improvement is not implemented for the additional regression ensemble, GAM, GPR and SVM models. These models show a mixed assortment of correlation. Regression ensemble, GAM and GPR show a good result within the training set, whereas the SVM model has significant issues at this stage. However, when introducing a non-training sorbent MOF-14, most of the models show significant error; the errors for the models are large enough to not provide a reasonable R-value. Some direct prediction and Freundlich isotherm models exhibit a fair correlation, but the R-values are less than an ideal 0.95. However, the Freundlich parameter predicted are used in an Aspen Adsorption bed model to examine the model response. The breakthrough times and recovery amounts vary among the different algorithms, with GPR and GAM showing the closest results. However, a comparison between the results of the parameters and the Aspen Adsorption model both indicate that the models have limited accuracy.

For future work, papers describing new adsorbents would ideally have additional information to remedy the small number of variables available. Theoretically, data imputation would be ideal to supplement and make more variables available; in practice, data imputation on the pore diameter has severe, significant issues in the resulting model. The data imputation performed was relatively simple regression ensemble using the other adsorbent properties to

predict the pore diameter, but the imputed variable actively hurts the capacity models. Including more robust variables can definitely improve both performance and generalization, as seen in the difficulties in helping with MOF-14. An idea of gathering more relevant information is to use commercially available adsorbents; these adsorbents usually come with data sheets that include physical and chemical information that can be used, such as chemical composition, density, and cell unit lengths & angles. ML methods are ideal in examining the underlying relationships between these and the adsorption process. Characterizing the performance of the adsorbents by other parameters such as cyclability will also be ideal in the future, but the lack of data makes this an effort far in the future.

Improving the performance of the Langmuir model is particularly important due to its prevalence in adsorption models. The Freundlich model, which is the best-performing model for MOF-14, is a much more difficult model to use. Within Aspen Adsorption, using the Freundlich isotherm results in significant stability issues; these issues are less present when the Langmuir isotherm is selected. It is also noted that the isotherm selection can have a large impact on the accuracy of the simulation. While Langmuir isotherm is simple and common, the gas components will interact with each other and the active sites, which is not in the model's assumptions. Instead, using models with more interaction factors can have greater accuracy; this must be carefully balanced with the increased number of parameters and thus the increased error introduced by each additional model. Moreover, generalizing these parameters will create a complex model that will need a large amount of new data to train any ML models. Another factor is to introduce other components for a more realistic simulation. In particular, post-combustion often have SO_x and NO_x which has operational problems that must be addressed.

The improvement of these models can have a significant impact as more interest begins to move towards the development phase. Determining the adsorbent performance from its textural properties can act as a strong guide towards the development of superior sorbents; additionally, with additional aide towards designing and researching, the model can provide more focus can be brought into the development stage.

Bibliography

[1] Environment and Climate Change Canada, "Greenhouse gas emissions," 2022. [Online]. Available: https://www.canada.ca/en/environment-climate-change/services/environmental-indicators/greenhouse-gas-emissions.html.

[2] A. I. Osman, M. Hefny, M. I. A. A. Maksoud, A. M. Elgarahy and D. W. Rooney, "Recent Advances in Carbon Capture Storage and Utilisation Technologies: A Review," *Environmental Chemistry Letter,* pp. 797-849, 2020.

[3] M. R. Rahimpour, M. Farsi and M. A. Makarem, Advances in Carbon Capture - Methods, Technologies and Applications, Cambridge, Massachusetts: Woodhead Publishing, 2020.

[4] A. L. Kohl and R. B. Nielsen, Gas Purification, 5th ed., Houston, Texas: Gulf Publishing Company, 1997.

[5] Ö. Yildirim, A. A. Kiss, N. Hüser, K. Leßmann and E. Y. Kenig, "Reactive absorption in chemical process industry: A review on current activities," *Chemical Engineering Journal,* pp. 371-391, 2012.

[6] W. Gaus, K. Hochschwender and W. Schunkck.United States of America Patent 1897725, 1933.

[7] J. Kittel and S. Gonzalez, "Corrosion in CO2 Post-Combustion Cpature with Alkanolaines - A Review," *Oil & Gas Science and Technology,* pp. 915-929, 2014.

[8] M. Minelli, S. Oradei, M. Fiorini and G. C. Sarti, "CO2 Plasticization Effect on Glassy Polymeric Membranes," *Polymer,* pp. 29-35, 2019.

[9] W. Guan, Y. Dia, C. Dong, X. Yang and Y. Xi, "Zeolite Imidazolate Frameworked (ZIF)-based Mixed Matrix Membranes for CO2 Spearation: A Review," *Journal of Applied Polymer Science,* 2020.

[10] Y. Liang, T. Kashdan, C. Sterner, L. Dombrowski, I. Petrick, M. Kröger and R. Höfer, "Algal Biorefineries," in *Industrial Biorefineries and White Technology*, Amsterdam, Elsevier, 2015, pp. 35-84.

[11] D. M. Ruthven, Principles of Adsorption and Adsorption Processes, New York: John Wiley & Sons, Inc., 1984.

[12] B. Crittenden and W. J. Thomas, Adsorption Technology & Desgin, Elsevier, 1998.

[13] M. Mofarahi and F. Gholipour, "Gas adsorption separation of CO2/CH4 system using zeolite 5A," *Microporous and mesoporous materials,* pp. 1-10, 2014.

[14] T. K. Prasad, D. H. Hong and M. P. Suh, "High Gas Sorption and Metal-Ion Exchange of Microporous Metal-Organic Frameworks with Incorporated Imide Groups," *Chemistry,* pp. 14043-14050, 2010.

[15] C. A. Grande and A. E. Rodrigues, "Electric Swing Adsorption for CO2 Removal from Flue Gases," *International Journal of Greenhouse Gas Control,* pp. 194-202, 2008.

[16] C. A. Grande, R. P. P. L. Ribeiro and A. E. Rodrigues, "Challenges of Electric Swing Adsorption for CO2 Capture," *ChemSusChem,* pp. 892-898, 2010.

[17] S. Gulati, Metal-Organic Frameworks (MOFs) as Catalysts, New Delhi: Springer, 2022.

[18] G. Zhu and H. Ren, Porous Organic Frameworks Design, Synthesis and Their Advanced Applications, Heidelberg: Springer, 2015.

[19] S. Choi, J. H. Drese and C. W. Jones, "Adsorbent Materials for Carbon Dioxide Capture from Large Anthropogenic Point Sources," *ChemSusChem,* pp. 796-854, 2009.

[20] C.-S. Ha and S. S. Park, Periodic Mesoporous Organosilicas: Preparation, Properties and Applications, Singapore: Springer, 2019.

[21] J. Friedman, R. Tibshirani and T. Hastie, The Elements of Statistical Learning: Data Mining, Inference, and Prediction, New York: Springer New York, 2009.

[22] H. A. Patel, J. Byun and C. T. Yavuz, "Carbon Dioxide Capture Adsorbents: Chemistry and Methods," *ChemSusChem,* vol. 10, pp. 1303-1317, 2017.

[23] M. Pardakhti, T. Jafari, Z. Tobin, B. Dutta, E. Moharreri, N. S. Shemshaki, S. Suib and R. Srivastava, "Trends in Solid Adsorbent Materials Development for CO2 Capture," *ACS Applied Materials & Interfaces,* vol. 11, pp. 34533-34559, 2019.

[24] X. Zhu, D. C. W. Tsang, L. Wang, Z. Su, D. Hou, L. Li and J. Shang, Machine learning exploration of the critical factors for CO2 adsorption capacity on porous carbon materials at different pressures, Elsevier, 2020.

[25] A. Lee and D. C. Miller, "A One-Dimensional (1-D) Three-Region Model for a Bubbling Fluidized-Bed Adsorber," *Industrial & Engineering Chemistry Research,* vol. 52, pp. 469-484, 2012.

[26] A. Ntiamoah, J. Ling, P. Xiao, P. A. Webley and Y. Zhai, "CO2 Capture by Temperature Swing Adsorption: Use of Hot CO2-Rich Gas for Regeneration," *Industrial & Engineering Chemistry Research,* vol. 55, no. 3, pp. 703-713, 2016.

[27] B. Chen, M. Eddaoudi, S. T. Hyde, M. O'Keeffe and O. M. Yaghi, "Interwoven metal-organic framework on a periodic minimal surface with extra-large pores," *Science,* vol. 291, pp. 1021-1023, 2001.

[28] J. R. Karra, B. E. Grabicka, Y.-G. Huang and K. S. Walton, "Adsorption study of CO2, CH4, N2, and H2O on an interwoven copper carboxylate metal–organic framework (MOF-14)," *Journal of Colloi and Interface Science,* vol. 392, pp. 331-336, 2013.

[29] D. W. Siderius, V. K. Shen, R. D. Johnson III and R. D. van Zee, NIST/ARPA-E Database of Novel and Emerging Adsorbent Materials, Gaithersburg: National Institute of Standards and Technology, 2023.

[30] P. I. Richards, On Game-Learning Machines, American Association for the Advancement of Science, 1952.

[31] M. Mofarahi and F. Gholipour, "Gas adsorption separation of CO2/CH4 system using zeolite 5A," *Microporous and Mesoporous Materials,* pp. 1-10, 2014.

Appendix A: GHG Emissions by Economic Sector in Canada

The data is publicly available from the Government of Canada.

Table A.1: GHG Emissions by Economic Sector in Canada

Year	Oil and gas	Transport	Buildings	Electricity	Heavy industry	Agriculture	Waste and others
1990	102.6	120.5	71.2	94.7	97.2	51.7	56.7
1991	102.2	114.3	70.6	96.1	97.1	52.3	55.3
1992	110.8	115.2	72.4	102.5	94.6	54.7	54.9
1993	117.5	116.7	76	93.1	94.1	56.5	53.7
1994	121.5	121.3	76.3	95.1	99.7	59.1	55.1
1995	127.6	122.1	77	98.2	100.4	62.2	57.9
1996	135.4	125.7	83.3	98.2	103.2	63.4	57.5
1997	136.5	131.5	80.8	109.4	102.6	64	57.5
1998	140.9	137.3	72.4	122.1	97.6	63.8	54.5
1999	149.9	143	76.3	119.1	94.7	63.5	55.2
2000	155.1	144.9	82.8	129	94.1	64.1	56.9
2001	156.6	146.6	79.5	129.2	88.3	62.9	55.2
2002	161.5	147.7	83.8	123.6	89	62.9	55.7
2003	165.9	151.7	89	127.3	88.3	65.1	55.9
2004	168.2	156.1	87.6	119	92.2	65.9	56.2
2005	171.3	160.1	83.7	117.5	87.2	66.4	55
2006	178	161	78.5	111.6	87	65	53.5
2007	183	164.4	84.3	119.6	86	65	54.5
2008	179.9	164.5	84.2	108.8	84.5	64.2	52.9
2009	176.9	161.5	82.6	93.7	71.5	61.9	49.5
2010	181.4	167.2	79.4	94.6	74.6	61.9	50.5
2011	187.2	168.3	84.7	86.6	80.4	62.4	51.3
2012	194.2	170.5	83.2	83.3	80.2	63.7	50.5
2013	198.9	174	84.3	79.7	78.6	65.4	51.3
2014	204.5	171.5	84.9	76.3	79.4	63.8	49.3
2015	204.8	172.1	83.8	79.7	77.8	64.6	49.8
2016	194.4	173.5	82.2	74.3	76.3	64.9	49.5
2017	196.5	178.9	86.6	72.6	75.5	64.3	50.5
2018	205	184.1	92.9	62.8	77.5	66.3	51.5
2019	203.5	185.5	92	61.8	77.4	66.7	51.5
2020	178.8	159.2	87.8	56.2	71.8	68.7	50

Appendix B: Aspen Adsorption Model Diagram

The following figures show the process diagram as well as the settings used.

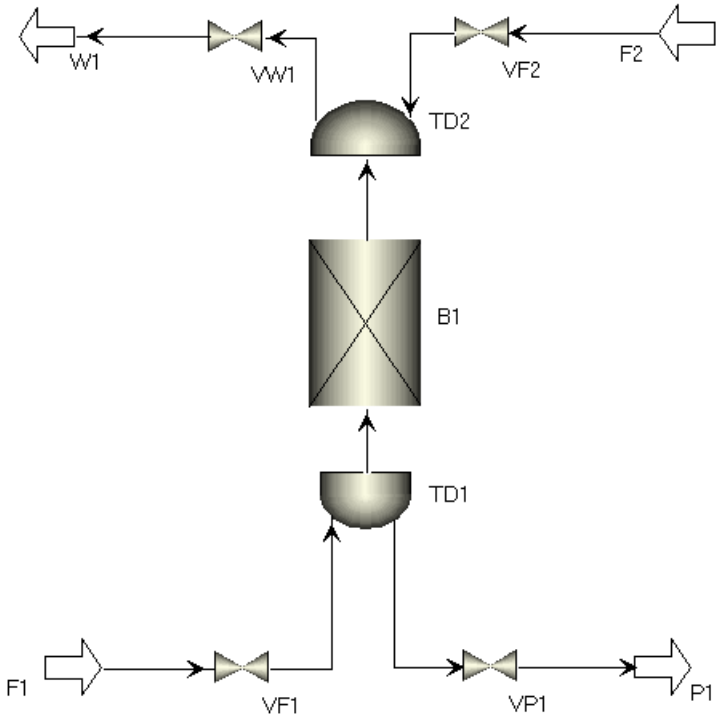

Figure B.1: Diagram of Aspen Adsorption Bed Model

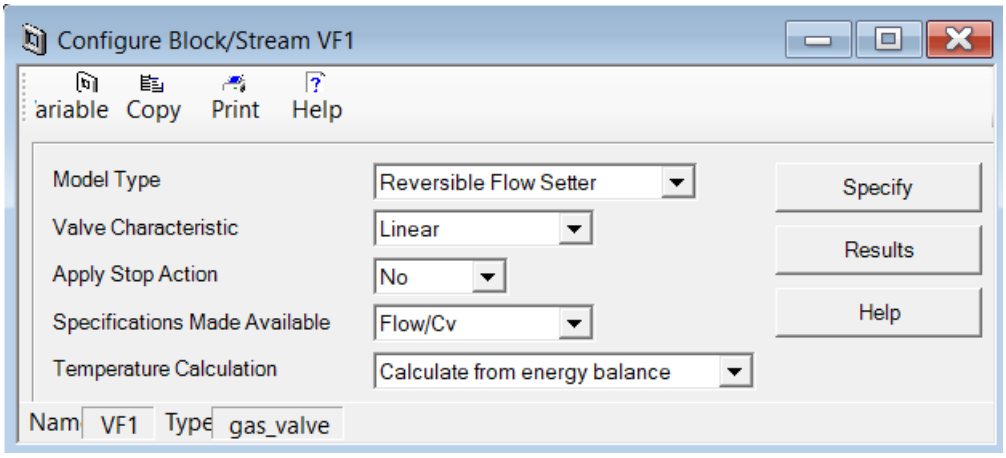

Figure B.2: Gas Valve Unit Configuration

Figure B.2 shows the configuration for the four gas_valve units VF1, VW1, VF2, VP1. The active specification of the valves is dependent on the cycle and shown in Table 2.1: Valve Staging

for Skarstrom Cycle. When VF1 is open, the flow rate is set to 0.0880624 mol/min. When VF2 is open, the flow rate is set to 0.0572407 mol/min. The two other valves VW1 and VP1 are on-off valves; the flow rate is controlled by the valves upstream and adsorption bed.

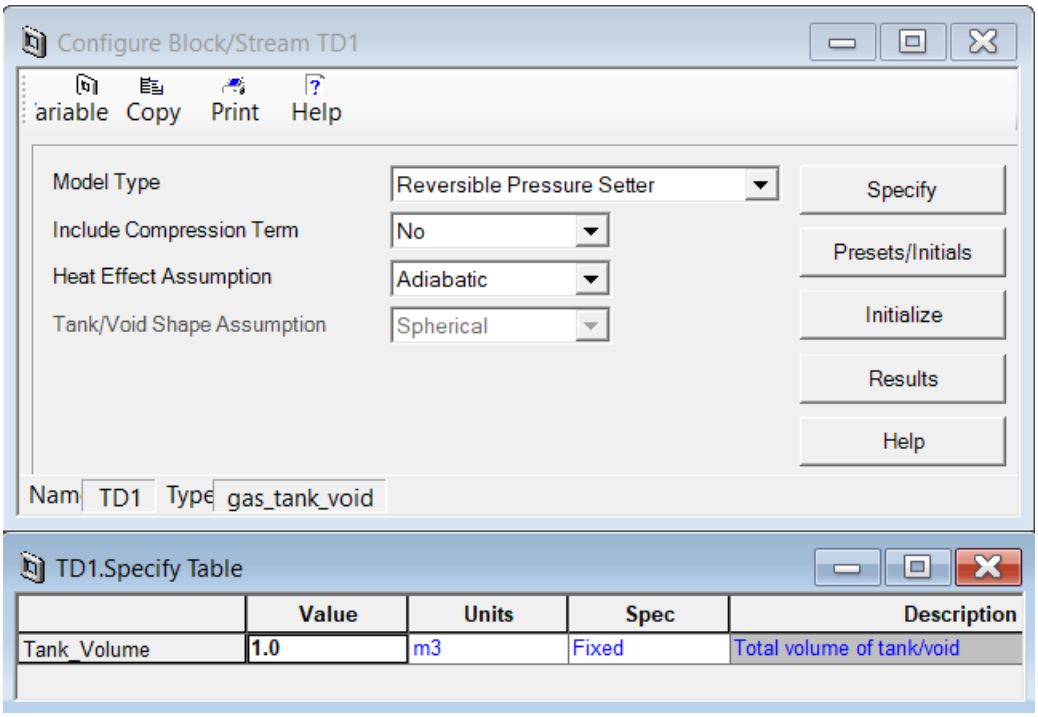

Figure B.3: Gas Tank Void Unit Configuration & Specification

The gas_tank_void units TD1 and TD2 are empty space to better facilitate the valves opening and closing. The compression term is removed for the blocks, as the compression of the gases causes instabilities in the temperature. As well, the tank volume has been changed to one cubic meter.

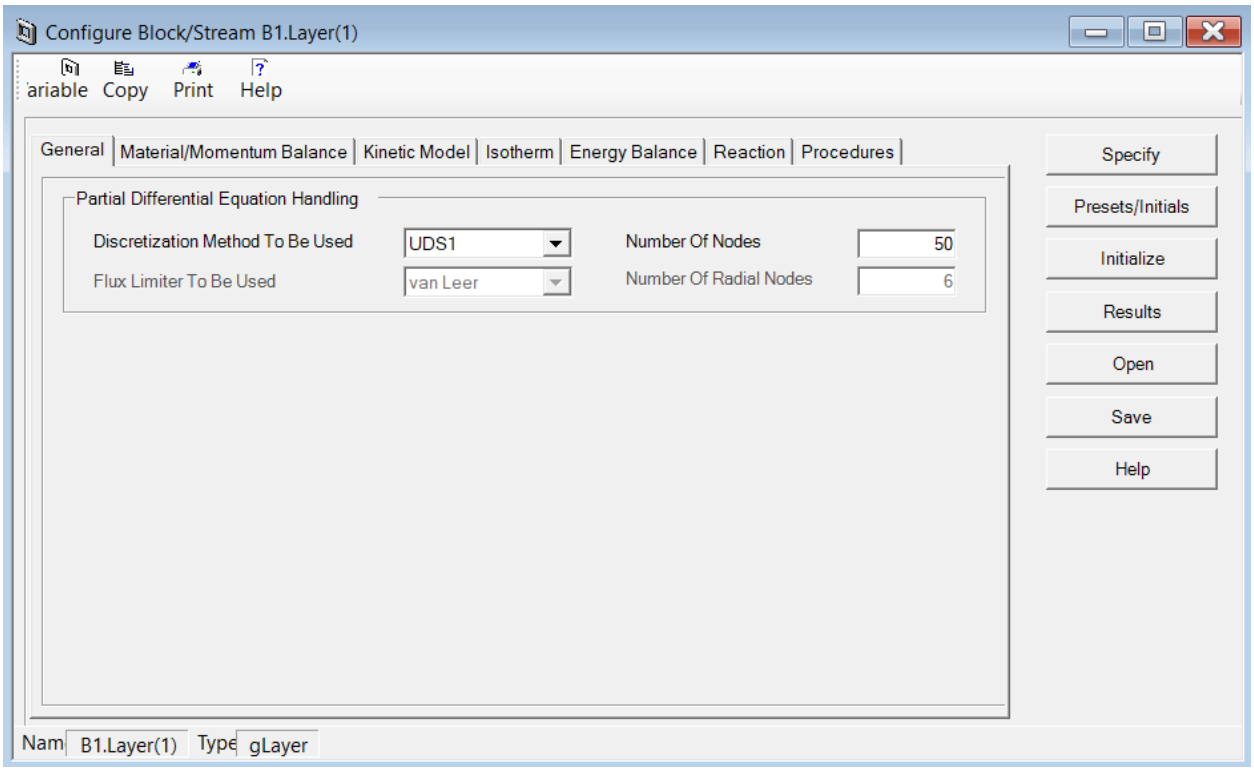

Figure B.4: PDE Handling Configuration

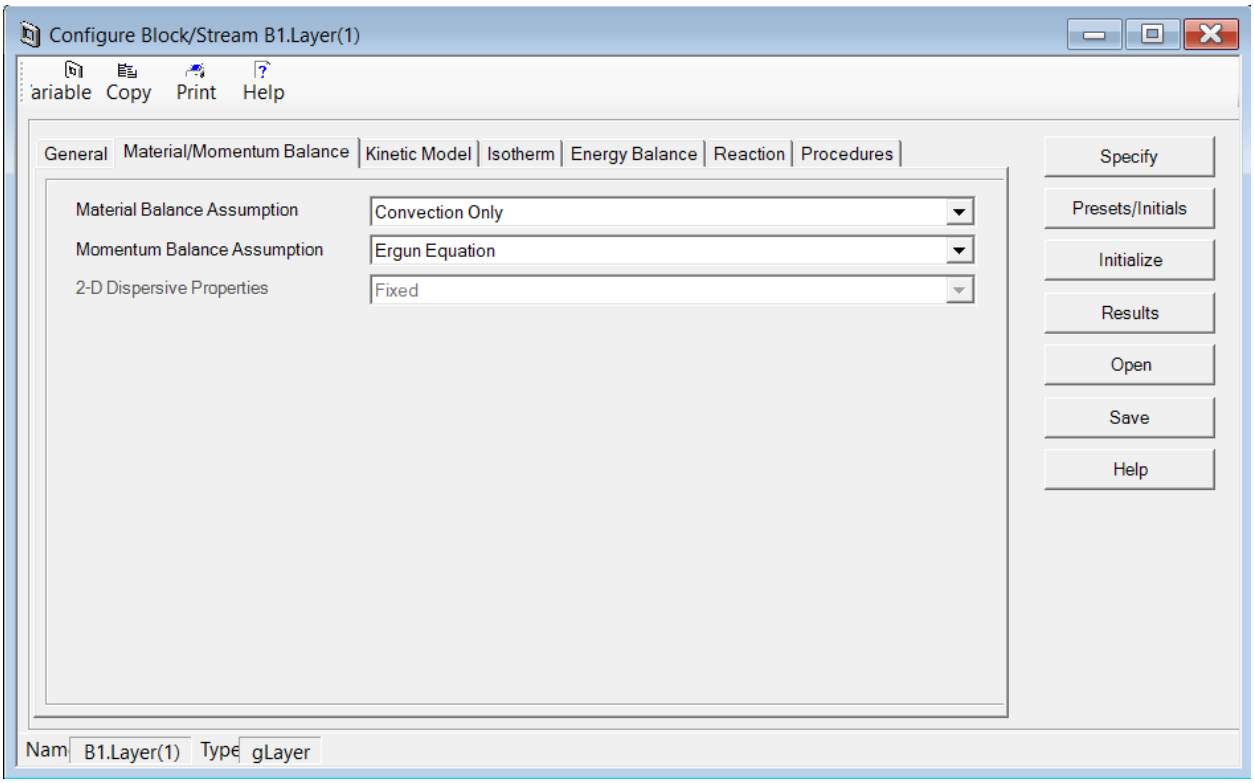

Figure B.5: Material/Momentum Balance Configuration

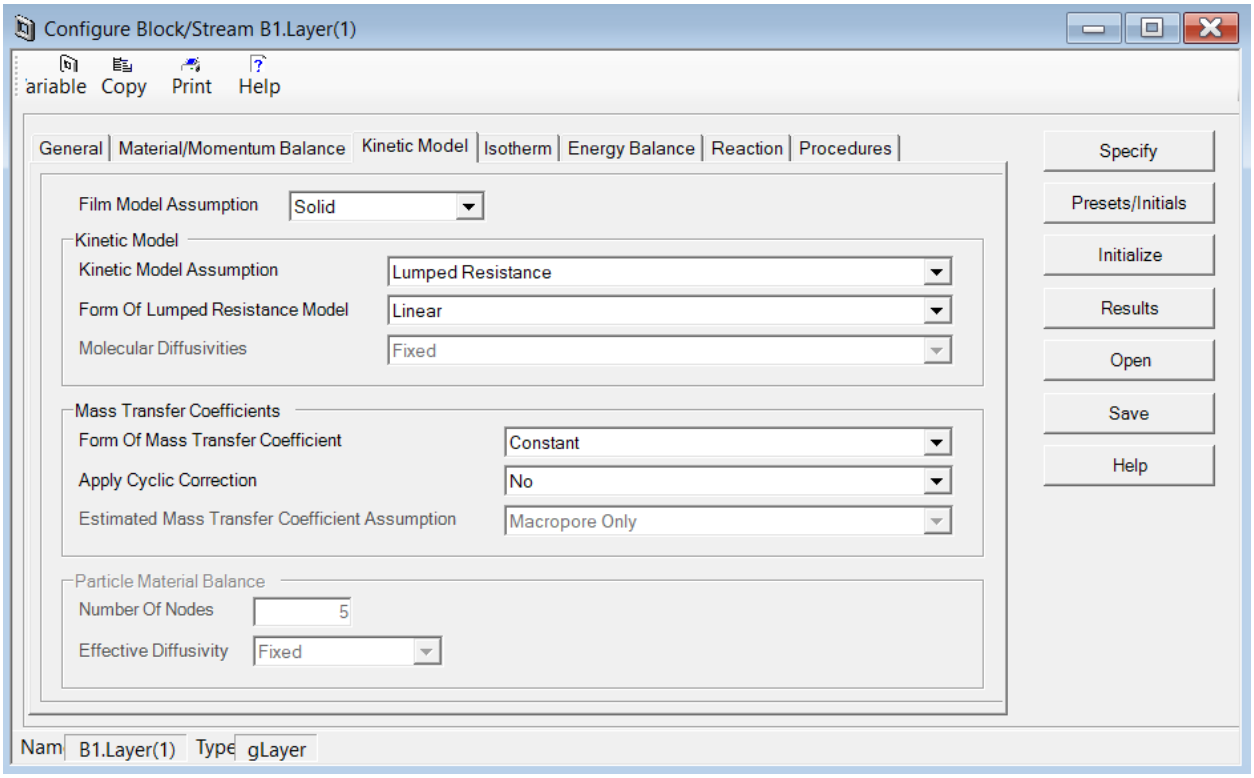

Figure B.6: Kinetic Model Configuration

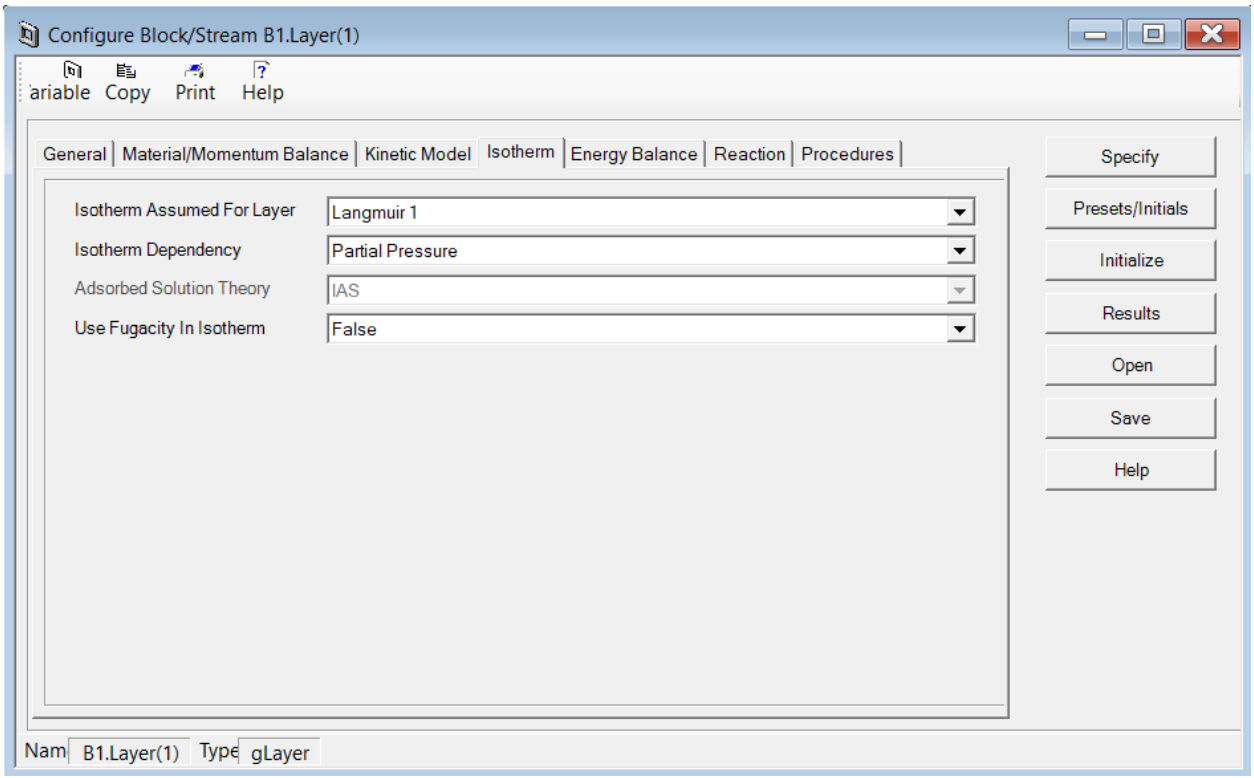

Figure B.7: Isotherm Configuration

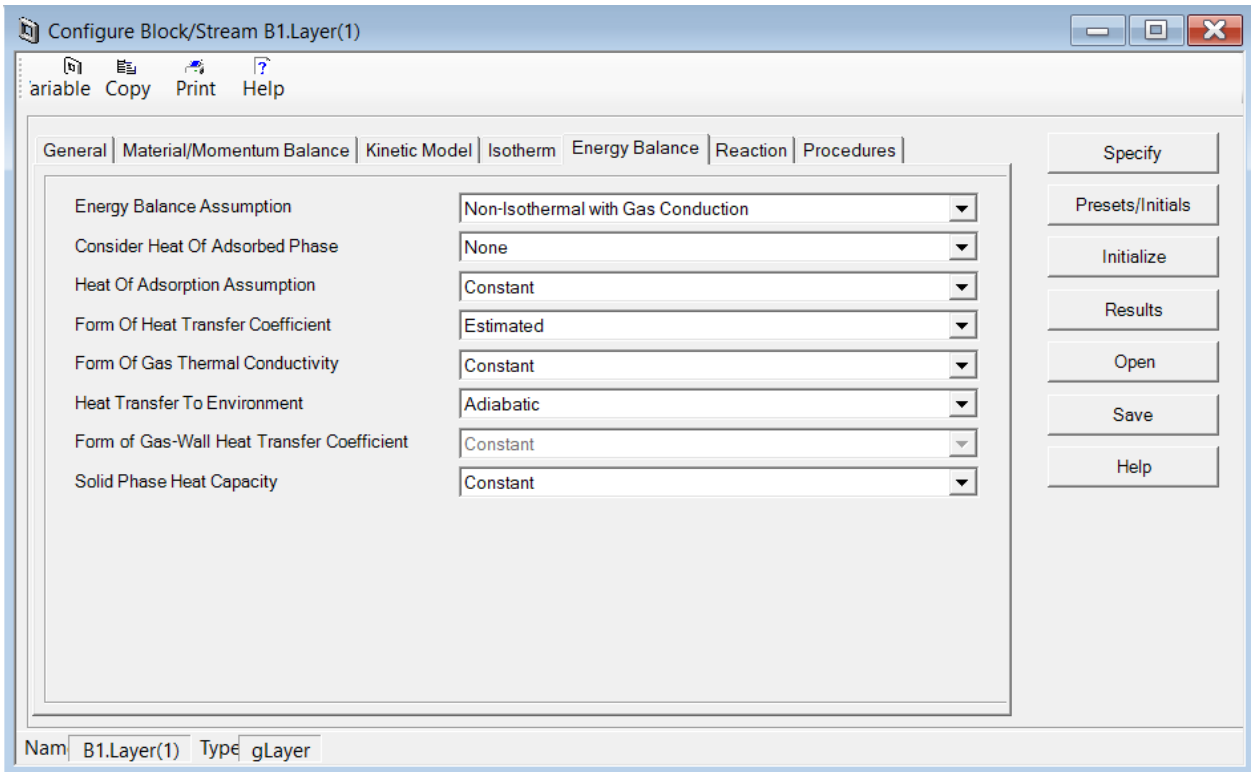

Figure B.8: Energy Balance Configuration

There are no reactions or user-defined procedures in the adsorption bed; no figures are created for this.